ISSN 2432-745X

Medical Mass Spectrometry

Vol. 8 No. 1, 2024

Guest Editor, Kaname Tsutsumiuchi

Japanese Society for Biomedical Mass Spectrometry

Medical Mass Spectrometry

Editorial Board

Editor-in-Chief

Makoto ARITA (Tokyo, Japan)

Associate Editors

Masayuki KUBOTA (Tokyo, Japan)
Fumio NOMURA (Chiba, Japan)
Daisuke SAIGUSA (Tokyo, Japan)
Masatoshi WAKUI (Tokyo, Japan)
Ikuko YAO (Sanda, Japan)
Yasuhiro MAEDA (Toyoake, Japan)
Tomoko OYA (Ichinomiya, Japan)
Emiko SATO (Sendai, Japan)
Seiji YAMAGUCHI (Shimane, Japan)

Editorial Board

Koutaro HASEGAWA (Hamamatsu, Japan)
Toyofumi NAKANISHI (Ichinomiya, Japan)
Mamoru SATOH (Tokyo, Japan)
Mitsutoshi SETO (Hamamatsu, Japan)
Kaname TSUTSUMIUCHI (Kasugai, Japan)
Kazuo IGARASHI (Kobe, Japan)
Toshimitsu NIWA (Ichinomiya, Japan)
Hiroshi SENO (Nagakute, Japan)
Yosuke SHIGEMATSU (Fukui, Japan)
Chunhua ZHANG (Yokohama, Japan)

International Advisory Board

Alma L. Burlingame (California, USA)
Dominic M. Desiderio (Tennessee, USA)
Neal Castagnoli (Virginia, USA)
Catherine Fenselau (Maryland, USA)

Published by Japanese Society for Biomedical Mass Spectrometry
Shubun University
6 Nikko-cho, Ichinomiya, Aichi 491−0938, Japan
E-mail: jsbms.office@gmail.com
Homepage: http://www.jsbms.jp/english/

Preface

The 48th Annual Meeting of the Japanese Society for Biomedical Mass Spectrometry

Kaname Tsutsumiuchi[1,*], Makoto Arita[2,3,4], Toshimitsu Niwa[5]

The 48th Annual Meeting of the Japanese Society for Biomedical Mass Spectrometry (JSBMS) was held on September 8th and 9th, 2023, at the WINC Aichi, Nagoya, Japan. Fortunately, we had a fruitful time discussing our latest studies face-to-face in the meeting, which could not be held for three years because of COVID-19. The program comprised three award lectures, three symposia with nine presentations, 46 short-oral and poster presentations, and two luncheon seminars.

This 8th issue of Medical Mass Spectrometry is based on the presentations at the 48th Annual Meeting of JSBMS (Nagoya).

The 49th Annual Meeting and the 3rd International Symposium of JSBMS and MSACL (Mass Spectrometry & Applications to the Clinical Lab) will be held on September 13th and 14th, 2024, organized by Prof. Ikuko Yao (Kwansei Gakuin University). We look forward to seeing you in Kyoto and exchanging information on medical mass spectrometry.

[1]College of Bioscience and Biotechnology, Chubu University
[*] E-mail: tsutsu@fsc.chubu.ac.jp
[2]Division of Physiological Chemistry and Metabolism, Keio University Faculty of Pharmacy
[3]Laboratory for Metabolomics, RIKEN Center for Integrated Medical Sciences
[4]Cellular and Molecular Epigenetics Laboratory, Graduate School of Medical Life Science, Yokohama City University
[5]Shubun University
Epub May 17, 2024.
DOI: 10.24508/mms.2024.06.005

Research Paper

DESI-IMS coupled with triple quadrupole mass spectrometry demonstrated the capability of NMN imaging in *Shelfordella lateralis* tissue

Zinat Tamannaa[1], Takumi Sakamoto[1], Md. Al Mamun[1], Soho Oyama[1], A.S.M. Waliullah[1], Ariful Islam[1], Md. Mahamodun Nabi[1], Shuhei Aramaki[1,2], Eisuke Tasaki[4,5], Yuki Mitaka[4,6], Mamoru Takata[4], Tomohito Sato[1,2], Tomoaki Kahyo[1,2], Kenji Matsuura[4], Mitsutoshi Setou[1,2,3]*

[1]Department of Cellular & Molecular Anatomy, Hamamatsu University School of Medicine, 1−20−1 Handayama, Higashi-Ku, Hamamatsu, Shizuoka 431−3192, Japan
[2]International Mass Imaging Center, Hamamatsu University School of Medicine, 1−20−1 Handayama, Higashi-Ku, Hmamatsu, Shizuoka 431−3192, Japan
[3]Department of Systems Molecular Anatomy, Institute for Medical Photonics Research, Preeminent Medical Photonics Education & Research Center, 1−20−1 Handayama, Higashi-Ku, Hamamatsu, Shizuoka 431−3192, Japan
[4]Laboratory of Insect Ecology, Graduate School of Agriculture, Kyoto University, Kitashirakawa-Oiwakecho, Sakyo-ku, Kyoto 606−8502, Japan
[5]Department of Life and Food Sciences, Graduate School of Science and Technology, Niigata University, 8050 Ikarashi 2-no-cho, Nishi-ku, Niigata 950−2181, Japan
[6]Department of Entomology, 2143 TAMU, Texas A & M University, College Station, Texas, 77843−2143, USA

Abstract Imaging mass spectrometry (IMS) has become an indispensable analytical tool for visualizing molecular distributions in biological tissues. However, the detection of many important biomolecules, such as nicotinamide mononucleotide (NMN) in tissue by IMS is still challenging due to their lower abundance. Although the sensitivity of widely used IMS instruments, desorption electrospray ionization (DESI) utilizing a time-of-flight (TOF) mass analyzer, is not sufficient to detect NMN in tissues, the recently developed DESI coupled with a triple-quadrupole (TQ) provides about ten times higher sensitivity than the DESI-Q-TOF. In this study, we first screened six insect species for NMN content using ultra-performance liquid-chromatography-tandem mass spectrometry (UPLC-MS/MS). Interestingly, *Shelfordella lateralis* showed significantly higher NMN content (15.5 mg/100 g of dry weight) than five other insect species used in this study. After screening, we tried to observe the distribution of NMN in *S. lateralis* using both DESI-Q-TOF and DESI-TQ, and only the DESI-TQ successfully detected the NMN in *S. lateralis.* DESI-TQ revealed prominent distributions of NMN in the abdomen of *S. lateralis* in selective reaction monitoring mode. To the best of our knowledge, this is the first report of NMN imaging in animal tissue applying IMS. Our study will contribute to the extended application of IMS for NMN imaging in mammalian tissues in the future. Furthermore, NMN imaging may help researchers to study nicotinamide adenine dinucleotide (NAD^+) metabolism in living organisms, which has significant implications for medical research and diagnosis.

Key words: IMS, NMN, DESI-TQ, DESI-Q-TOF, UPLC-MS/MS, *Shelfordella lateralis*

***Corresponding author**
Mitsutoshi Setou
Department of Cellular & Molecular Anatomy, Hamamatsu University School of Medicine, 1−20−1 Handayama, Higashi-ku, Hamamatsu, Shizuoka 431−3192, Japan
Tel: +81−53−435−2086, Fax: +81−53−435−2468
E-mail: setou@hama-med.ac.jp
Received: August 16, 2023. Accepted: January 11, 2024.
Epub April 19, 2024.
DOI: 10.24508/mms.2024.06.001

Introduction

Imaging mass spectrometry (IMS) has been increasingly used to visualize biomolecules due to its high sensitivity and label-free nature. This technology has made it possible to reveal the identity and distribution of the specific molecule and the localization of the molecule in organs[1)]. Nowadays, imaging with desorption electrospray ionization (DESI), in combination with quadrupole-time-of-flight

(Q-TOF) mass spectrometry, has been gaining much popularity for visualizing molecular distribution on a sample surface under ambient conditions[2]. DESI-Q-TOF has shown the capability of visualizing spatial distributions of molecules with diverse chemical natures, such as small molecules[3], free fatty acids[4–6], phospholipids[7], lipid biomarker[8], active compounds[9], and other metabolites[10]. One of the significant advantages of DESI-IMS is that it requires a minimal sample preparation than traditional mass spectrometry, such as matrix-assisted laser desorption ionization mass spectrometry (MALDI-MS)[11]. Recently, DESI combined with triple quadrupoles (TQ) mass spectrometry has emerged and offers advantages over DESI-Q-TOF. The TQ mass analyzer consists of three quadrupole mass filters, while DESI-Q-TOF consists of a single quadrupole mass filter. These three quadrupole mass filters make DESI-TQ more specific for precursor-to-product ion transitions of the targeted compound analysis[12]. This allows DESI-TQ to exhibit higher specificity and excellent sensitivity in selective reaction monitoring (SRM) mode than other high-resolution mass analyzers[13].

Despite the significant improvements in the sample preparation and instrumentations of IMS, detecting and imaging of many biologically important molecules in tissue is still challenging. For example, nicotinamide mononucleotide (NMN), a well-known vital precursor of nicotinamide adenine dinucleotide (NAD^+), has been found difficult to be detected by IMS. The analytical detection of NMN is challenging due to its physicochemical characteristics[14]. NMN is a nucleotide containing a pyridine base. It is an acid- and water-soluble nucleotide found in all living cells as a coenzyme. Increasing NAD^+ levels improves insulin sensitivity, reverses mitochondrial dysfunction, and enhances lifespan[15]. When taken orally, NMN is quickly absorbed and converted into NAD^+[16]. NAD^+ availability is essential for slowing the aging process[17]. Oral nicotinamide supplementation within the daily acceptable upper threshold is an efficient strategy to raise NAD^+ levels and influence blood lipid composition[18]. Thus, NMN has important applications in medicine and healthcare[19], but the chemical synthesis of NMN is complex[20]. Therefore, it is worth exploring a rich source of natural NMN and its imaging in medical research.

Unlike other natural products, insects have received comparatively little attention in imaging studies as sources of modern medicines[21]. Insects can provide proteins for human use, and people in many parts of the world consume insects as a potential source of calories and protein[22]. In traditional folk medicine and Chinese medicine, the whole body extracts of several bees, wasps, flies, butterflies, moths, cockroaches, beetles, and other insects act as antiviral, antibacterial, and anti-cancer agents[21]. While insects are consumed as food in various cultures around the world and are known to be rich in protein and nutrients, there is not adequate knowledge or research about their NMN content.

Recently, our group has explored high NMN content in *Cinnamomum verum J. Presl* bark, a medicinal plant, using liquid chromatography mass spectrometry (LC-MS)[23]. Applying the same method, we first screened NMN content in six insect species in this study, namely, the Turkestan cockroach *Shelfordella lateralis*, the field cricket *Gryllus bimaculatus*, the damp-wood termite *Hodotermopsis sjostedti*, the black soldier fly *Hermetia illucens*, the Japanese subterranean termite *Reticulitermes speratus*, and the giant mealworm *Zophobas atratus*. Finally, we employed both DESI-Q-TOF and DESI-TQ to observe the distribution of NMN in *S. lateralis* bodies, which showed the highest NMN content among the other species under this study.

Materials and Methods

Chemicals and reagents

We purchased the standard β-nicotinamide mononucleotide (β-NMN) from Tokyo Chemical Industry Co. (Tokyo, Japan). LC/MS-grade formic acid (99%), acetonitrile (ACN), methanol, ethanol, and ultra-pure water were obtained from Fujifilm Wako Pure Chemical Corporation, Ltd. (Osaka, Japan). Ammonium format solution was purchased from Kanto Chemical Co., INC. (Tokyo, Japan). Sodium formate was obtained from Sigma-Aldrich Co. LLC (St. Louis, MO, USA) and, leucine enkephalin from Waters Corporation (Milford, MA, USA).

Sample preparation for the quantification of NMN

Two types of termite species (*H. sjostedti*, *and R. speratus*) were used in this study. *H. sjostedti* were collected initially from logs from brown-rotted Luchu pine wood (*Pinus luchuensis*) in the forest of Amami Oshima Island in Japan. And the colonies of *R. speratus* were collected from logs from brown-rotted cedar wood (*Cryptomeria japonica*) in the forest in Kyoto, Japan. The termite colonies were maintained at the Laboratory of Insect Ecology, Kyoto University, at about 25°C under dark. The Individuals of *H. sjost-*

edti were randomly extracted from each of the six colonies (colony code: KM022, KM024, KM025, KM103, KM109, TMK091). And the individuals of *R. speratus* were randomly extracted from each of the three colonies (colony code: MT616D, MT617E, and MT619G). We bought the cockroach *S. lateralis* from Rakuten Group, Inc., Tokyo, Japan, and the freeze-dried *G. bimaculatus* from Leaf Corporation, Gunma, Japan. The two other insect species, dried *H. illucens*, and dried *Z. atratus*, were purchased from GEX Corporation, Osaka, Japan, and Sanko-Tokai Co., Ltd., Osaka, Japan, respectively.

All the samples were kept in a −80°C freezer until freeze-dried treatment. The frozen insect samples were freeze-dried (Freeze Dryer FD-1000, EYELA, Bunkyo, Tokyo, Japan) and ground (Wonder Crusher WC-3 L, Osaka Chemical Co. Ltd., Kita, Osaka, Japan) to form a powder. The resulting insect powder (each about 5 g) was respectively vacuum-sealed (Impulse Vacuum Sealer V301G-10WK, FUJIIMPULSE Co. Ltd., Toyonaka, Osaka, Japan) and kept in −20°C freezer until use for analyses.

Standard sample preparation

For standard sample preparation, an analytical balance (AUY220, SHIMADZU, Kyoto, Japan) was used to weight the NMN standards. Then, 25% ethanol was used to dissolve the NMN standard. The prepared NMN standard was then serially diluted to control solutions at concentrations of 500, 200, 100, 50, and 20 ng/mL for calibration curve preparation.

Insect extract preparation for UPLC-MS/MS

For each sample, approximately 50 mg of powder was weighed three times. Then 25% ethanol was added (40 μL/mg of the sample) and extracted for one minute on ice with a mechanical homogenizer (HK-1, AS ONE, Osaka, Japan) at 9000 rpm. The homogenized insect extracts were then centrifuged for 10 minutes at 3000 rpm in 4°C. Then the supernatant was filtered through a 0.42 μm filter, and the cleared sample was transferred to LC-MS vials.

UPLC-MS/MS analysis

ACQUITY (UPLC H-Class PLUS, Waters) coupled with a triple quadrupole mass spectrometer (Xevo TQ-XS, Waters) was used to analyze the insect extracts. An Intrada Amino Acid column (3 μm, 3.0×100 mm, Imtakt) was carried out for chromatographic separation, which was kept at 40°C throughout the measurement. The electrospray ionization (ESI) source was used on the mass spectrometer, and the analysis was performed in positive ion mode. The capillary voltage was set to 3.5 kV, the cone voltage to 22 V and the source temperature was 150°C. The desolvation temperature was fixed at 500°C and the desolvation gas flow rate was 600 L/h. The cone and nebulizer gas flows were set to 150 L/h and 7.0 Bar, respectively. Mobile phase A consisted of 0.3% formic acid in ACN, while mobile phase B was acetonitrile/100 mM ammonium formate (20:80, v/v). The flow rate used for elution was 0.6 mL/min. The following setup was used to perform the gradient elution procedure: 0 to 0.5 min, 20% B; 0.5 to 2.5 min, 20% to 100% B; 2.5 to 4.5 min, 100% B; 4.5 to 4.6 min, 100% to 20% B; 4.6 to 7.0 min, 20% B. The whole duration of the run time was 7 min. An aliquot of 5 μL of the prepared sample was injected into the system while the autosampler was kept at a constant temperature of 10°C. The SRM transition from *m/z* 335.1 to *m/z* 123.0 using a collision energy of 10.0 eV was used for NMN quantification.

A MassLynx software (Waters, version 4.1) was used to acquire and analyze the UPLC-MS/MS data, and, TargetLynx software (Waters, version 4.1) was used for the quantitative measurement. The statistical analysis was carried out using GraphPad Prism (version 8.42).

Sample preparation for DESI-IMS analysis

After collecting the samples, the whole body of the cockroach was embedded overnight by a super cryo-embedding medium in the middle of a cryomold and frozen at −20°C. The frozen cockroach samples were then mounted on a sample holder using the optimal cutting temperature (OCT) compound (Sakura Finetek Japan, Tokyo, Japan). The tissues were sectioned sagittally at 20 μm thickness at −20°C by a cryostat system (CM1950; Leica Biosystems, Wetzlar, Germany). Then the sections were mounted on glass slides (Matsunami, Osaka, Japan) and stored at −80°C. Before DESI-IMS analysis, the slices were air-dried.

DESI-Q-TOF analysis

DESI-IMS analysis was performed in positive ion mode using DESI source attached to a Q-TOF mass analyzer (Xevo G2-XS Q-TOF, Waters). Before the measurements, sodium formate solution (500 μM) in 2-propanol: water (90:10, v/v) was used to calibrate the mass spectra externally, and leucine enkephalin solution (500 μM) was used

to set up the detector. A solvent pump (ACQUITY UPLC Binary Solvent Manager, Waters) was used to deliver the spray solvent (98:2 methanol/water, v/v) at a flow rate of 2 μL/min. A 2D sampling stage was equipped with a DESI source to scan the designated area with a scan rate of 200 μm/sec, and the pixel size was 100 μm × 100 μm. The DESI source conditions were optimized using the following parameters: a nebulizing nitrogen gas pressure of 0.4 MPa, a capillary voltage of 4.0 kV, a spray impact angle of 70°, a sampling cone of 50, and an inlet temperature of 120°C. The setup for mass resolution, mass window, and collision energy were at 20000, 0.02 Da, and 4.00 V. The mass spectra were collected using a mass range of *m/z* 100 to 1000 of the 1000 peaks with the highest intensities. The data were then further processed at the range of *m/z* 300 to 400 to detect the ion images of lower intensities.

DESI-Q-TOF data were acquired and processed using the MassLynx software (Waters, version 4.1). And, HDI Imaging software (Waters, version 1.4) was used to analyze the ion images.

DESI-TQ analysis

A Xevo TQ-XS equipped with a DESI source (Waters) has been employed for imaging in SRM mode. A syringe pump delivered the DESI-IMS solvent ($MeOH/H_2O$, 98/2, v/v) at a flow rate of 2 μL /min. For NMN imaging, the DESI source conditions were optimized using the following parameters: N_2 nebulizing gas pressure of 0.8 Mpa; capillary voltage of 0.85 kV (Positive); MS source temperature of 150°C; sampling cone voltage of 20 V. The distances between the emitter tip and the surface, the mass inlet and the surface, and the mass inlet were roughly 2, 6, and 0.5 mm, respectively. The identified areas on the glass slide were scanned at a scan rate of 10 scan/sec. The pixel size was set as 50 μm × 50 μm for tissue and 100 μm × 100 μm for standard. A collision energy of 20 eV was used for NMN transition (*m/z* 335.1 to *m/z* 123.0). The SRM dwell time was set as 0.0016 sec/pixel. At least two serial sections of the cockroach sample were analyzed under the same experimental conditions. Following the measurement, tissue sections were stained with hematoxylin and eosin (H&E) for histological analysis.

The ion image of DESI-TQ data was acquired and processed using the updated version of MassLynx (Waters, version 4.2) software and HDI Imaging (Waters, version 1.6) software.

Results

In this study, we first conducted a quantification study of NMN in six different insect species *S. lateralis*, *G. bimaculatus H. sjostedti*, *H. illucens*, *R. speratus*, and *Z. atratus* by LC/MS (Fig. 1b). As seen in Fig. 1a, a linear calibration curve (Y=9.3056X−154.914, R=0.99) of NMN standards was observed in the range of 20−500 ng/mL. Chromatograms showed the clear detection of NMN standard at each point (Fig. S1a−e).

A Chromatogram of NMN (SRM transition at *m/z* 335.1 to *m/z* 123.0) was observed with high intensities in *S. lateralis*, *G. bimaculatus* (Fig. 1b, Fig. S2a−b), *H. sjostedti*, *H. illucens* (Fig. 1b, Fig. S3c−d), and *R. speratus* (Fig. 1b, Fig. S4e). On the other hand, NMN was not detected in the species of *Z. atratus* (Fig. 1b, Fig. S4f). The average concentration of NMN in *S. lateralis*, *G. bimaculatus*, *H. sjostedti*, *H. illucens*, and *R. speratus* were 15.5, 6.93, 3.01, 0.143, and 0.13 mg/100 g (dry weight) respectively. *S. lateralis* showed significantly higher NMN content than all other species in this study ($p<0.0001$) (Fig. 2). *G. bimaculatus* showed the second highest content of NMN, which was significantly higher than *H. illucens*, *R. speratus*, and *Z. atratus* ($p<0.005$) (Fig. 2).

For the imaging study, we first performed DESI-Q-TOF analysis in the whole body of *S. lateralis*. But we could not detect NMN in the entire body of *S. lateralis* (Fig. S5a), we could only detect NMN at *m/z* 335.1 $[M+H]^+$ in NMN standard (20 μg/mL) (Fig. S5a). In this analysis, NMN was not detected with other adducts in both NMN standard and *S. lateralis* (Fig. S5b).

Next, we performed DESI-TQ in the SRM mode to see the distributions of NMN in the sagittal sections of whole-body *S. lateralis*. NMN (SRM transition of *m/z* 335.1 to *m/z* 123.0) was successfully detected in almost entire regions of the *S. lateralis* section (Fig. 3b). To observe the region-specific distribution of this molecule in *S. lateralis*, the histological images were overlaid on the ion image (Fig. 3c). Interestingly, NMN was notably higher in some specific parts of the *S. lateralis* abdomen, possibly in the midgut. For further confirmation of the NMN assignment, pure NMN solution (1 μg/mL) and extract from dry *S. lateralis* were spotted on the same slide and measured subsequently. As expected, the ion images at the same NMN transition were clearly detected for pure NMN (Fig. 3d) and the *S. lateralis* extract (Fig. 3e).

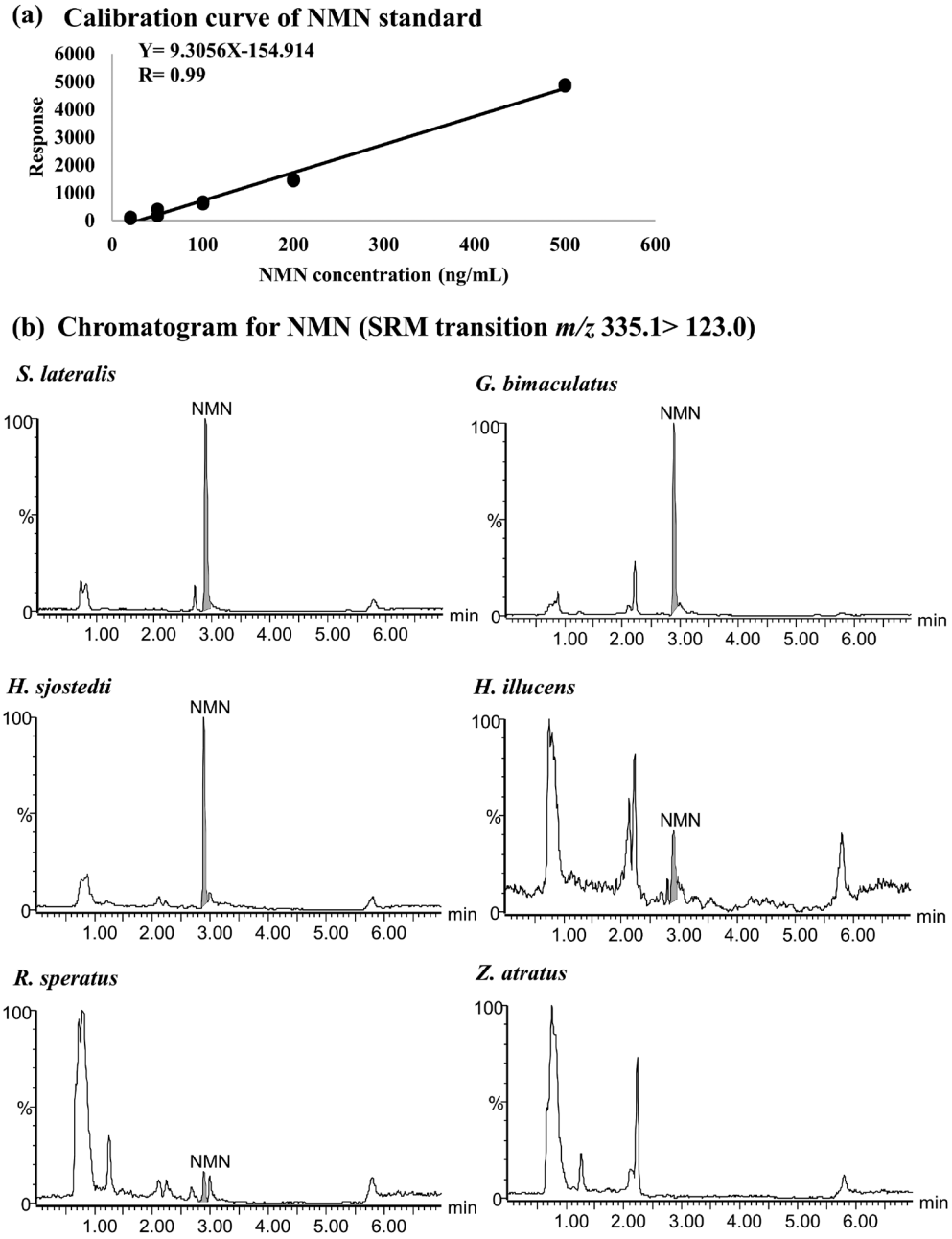

Fig. 1. Calibration curve of NMN standards (a) and representative chromatogram of NMN obtained from six different species of insects (b).

Discussion

For the first time, in this study, we demonstrated the NMN imaging in biological tissue employing DESI-TQ in SRM mode that showed higher sensitivity and excellent selectivity than DESI-Q-TOF. Detection of NMN in tissue is challenging by IMS since this molecule is very labile and readily undergoes in-source fragmentation under standard electrospray ionization settings[24]. DESI-Q-TOF is typically used for untargeted analysis where the target ion is mixed with myriads of other ions and could not be detected. In our experience, DESI-TQ provides about ten to a thousand times higher sensitivity than the DESI-Q-TOF. In this study, DESI-TQ successfully detected NMN in *S. lateralis* (Fig. 3), which could be attributed to its improved sensitivity. It is to be noted that the sensitivity of DESI-TQ is influenced by various factors, including dwell time. Dwell time refers to the duration the mass spectrometer spends analyzing a particular ion in a particular spot on the sample surface. Increasing dwell time leads to higher sensitivity as the instrument has more time to accumulate ions from the sample. However, longer dwell times can compromise spatial resolution. This is because the instrument spends more time

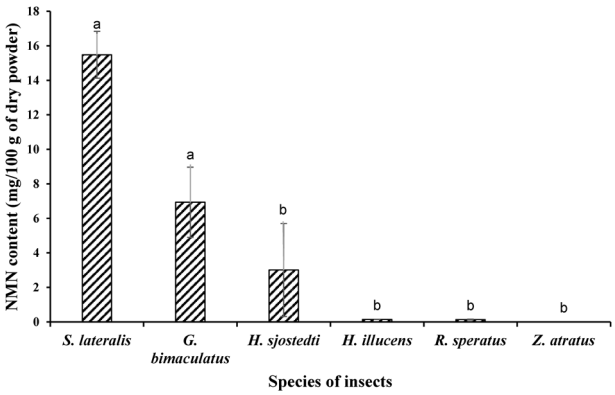

Fig. 2. Comparison of NMN content among different species of insects.
Different letters indicate a significant difference ($p < 0.01$) among different species. One-way ANOVA was performed followed by Tukey's multiple comparison tests among different species of insects. All the data are represented as mean±SD. The same insect samples were prepared in triplicate.

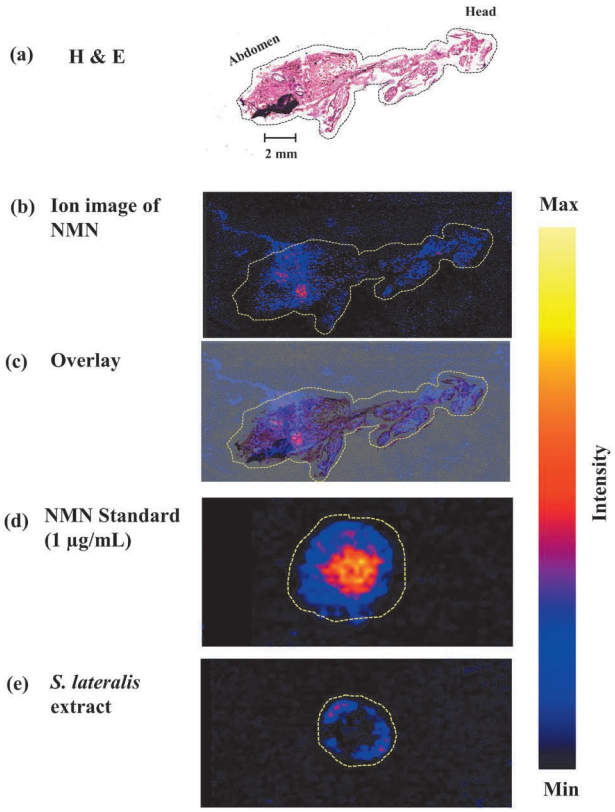

Fig. 3. Distribution of NMN in the whole body of *S. lateralis by* DESI-TQ.
H&E images of *S. lateralis* section (a). Representative DESI-IMS ion image for NMN (SRM transition at *m/z* 335.1 to *m/z* 123.0) in *S. lateralis* section (b), NMN standard (d), and *S. lateralis* extract (e). Transparent overlaid images between H&E and ion images for NMN in *S. lateralis* (c).

at each spot, resulting in a larger area being sampled, which may reduce the ability to discriminate features at a finer spatial scale. Therefore, finding the optimal balance between dwell time, sensitivity, and spatial resolution is recommended.

The analysis of insects, such as *S. lateralis*, by IMS presents inherent challenges. Ideally, freezing the sample immediately after sacrificing the animal or insect is crucial to prevent post-mortem degradation of certain analytes. However, the delicate anatomical structure of *S. lateralis* poses difficulties in cryo-sectioning fresh-frozen samples without using an embedding medium. To address this issue, we employed a super cryo-embedding medium for the entire body of *S. lateralis*. This approach facilitates cryo-sectioning without compromising the mass spectral quality, thanks to the medium's monomeric property. It is important to note that freezing samples using cryo-embedding medium requires a longer time compared to direct freezing, this procedure may impact the imaging of certain biomolecules susceptible to rapid post-mortem degradation. Fortunately, there is no reported literature on the post-mortem degradation of NMN, supporting the compatibility of NMN imaging in frozen and embedded samples.

One of the challenges in NMN imaging is the potential delocalization during sample preparation. In our experience, NMN delocalization was observed when tissue section was stored in the freezer before analysis. This is because NMN is highly soluble in water. In our study, we dried the sample immediately after cryo-sectioning to minimize the NMN delocalization. Previously MALDI-IMS was used for peptide imaging in formalin-fixed and paraffin-embedded (FFPE) *S. lateralis*[25]. However, FFPE samples are not suitable for NMN imaging since they require deparaffinization and extensive washing procedure.

Our group recently developed a rapid SRM method (7 min run per injection) to screen and quantify NMN in plant extract using UPLC-MS/MS[23]. SRM has been a gold standard for quantification studies. We employed the same method in our current study and found a significantly higher content of NMN in *S. lateralis* compared to other species of insects. Cockroaches are one of the most successful and diverse insects in traditional and Chinese medicine[26]. Previously Miles et al. investigated NMN content in various natural raw foods, including edamame, broccoli, cucumber seed, cucumber peel, cabbage, avocado, tomato, mushroom, beef, and shrimp. Among these, edamame

showed the highest content of NMN (0.47−1.88) mg/100 g[27]. Considering the moisture content (60−65%)[28], the NMN content in edamame should be approximately 1.18−4.7 mg/100 g dry weight. In contrast, cockroaches have an NMN content of 15.5 mg/100 g dry weight (Fig. 2), about 3 to 13 times higher than edamame. This is the first study that revealed the surprisingly higher content of NMN in insects. Cockroach extracts have been used for centuries to treat aches, pains, inflammation, and even chronic heart failure[29]. The gut microbial metabolites of cockroach is a valuable source of new bioactive compounds with therapeutic promise for human health[26]. Our study also indicated the promising use of this insect, particularly in pharmaceuticals. A recent study found that milk from cockroach species had a higher potential for nutrition than milk from typical mammals[30]. As a result, it is thought of as a potential new superfood that might be made accessible for ingestion shortly. It is to be noted that cockroaches carry food-borne pathogens that may transmit diseases to humans[31]. Therefore, more research is required to focus on the sanitation and safety of cockroaches.

In our study, the second higher amount of NMN was present in *G. bimaculatus*. This insect species is used as food and feed[32]. A previous study showed that the extract of *G. bimaculatus* can treat aging in the WKY mice model by dramatically lowering creatinine phosphokinase levels in the serum[33]. We also found a significant amount of NMN in *G. bimaculatus*, suggesting it might have a potential role in anti-aging. We have analyzed two species of termites, *R. speratus*, and *H. sjostedti*. In our investigation, the third higher amount of NMN was present in *H. sjostedti*. Termites are eusocial insects used as model organisms in aging research[34]. Recently, DESI-IMS analysis of ^{13}C-labeled termites revealed that the royal diet contained phosphatidylinositol and acetyl-L-carnitine, which are known to be anti-aging agents[35] and this may explain termite royals' remarkable longevity in eusocial insects[36]. This fact strongly suggests that termites have anti-aging agents in their bodies, and therefore, NMN may also be involved in the longevity of *H. sjostedti*.

Our study has some limitations. We could not assign the anatomical region of *S. lateralis* unambiguously where NMN exhibited high distribution. The current data did not explore the potential post-mortem degradation of NMN within the *S. lateralis*.

In conclusion, the current study demonstrated the NMN imaging in tissue by DESI-TQ and revealed *S. lateralis* as a rich source of NMN, specifically in the abdomen. We believe that, our method will help to develop other animal imaging in the field of biomedical research. In the future, NMN imaging could aid in understanding age-related changes in NAD^+ metabolism and its potential role in human health.

Acknowledgment

This work was supported by the Cabinet Office, Government of Japan, Moonshot Research and Development Program for Agriculture, Forestry and Fisheries (funding agency: Bio-oriented Technology Research Advancement Institution) Grant number JPJ009237 (to K.M.), JSPS KAKENHI (Grant Number JP18H05268 to K.M.), and JSPS KAKENHI (Grant Number JP23H69332 to K.M.).

Conflicts of Interest

The authors declare no conflict of interest.

References

1) Saito Y, Eto F, Takei S, Yao I, Setou M: Imaging mass spectrometry reveals sodium lauryl sulfate induced changes in skin lipoquality, principally affecting sphingomyelin. *Med Mass Spectrom* 3: 35−42, 2019.
2) Shimma S: Mass spectrometry imaging. *Mass Spectrom* 11: 1−15, 2022.
3) Waliullah A, Sakamoto T, Uchiyama T, Itai E, Naru E, et al: Detection of highly abundant small molecules in the stratum corneum of healthy young women using desorption electrospray ionization mass spectrometry imaging. *Med Mass Spectrom* 7: 26−34, 2023.
4) Al Mamun M, Sato S, Naru E, Sakata O, Hoshikawa E, et al: Higher accumulation of docosahexaenoic acid in the vermilion of the human lip than in the skin. *Int J Mol Sci* 21: 2807, 2020.
5) Takeyama E, Islam A, Watanabe N, Tsubaki H, Fukushima M, et al: Dietary intake of green nut oil or DHA ameliorates DHA distribution in the brain of a mouse model of dementia accompanied by memory recovery. *Nut* 11: 2371, 2019.
6) Sato T, Horikawa M, Takei S, Yamazaki F, Ito TK, et al: Preferential incorporation of administered eicosapentaenoic acid into thin-cap atherosclerotic plaques. *Arterioscler Thromb Vasc Biol* 39: 1802−1816, 2019.
7) Islam A, Takeyama E, Mamun M. Al, Sato, T., Horikawa,

M., et al: Green nut oil or DHA supplementation restored decreased distribution levels of DHA containing phosphatidylcholines in the brain of a mouse model of dementia. *Metabolites* 10: 4, 153−164, 2020.

8) Tamura K, Horikawa M, Sato S, Miyake H, Setou M: Discovery of lipid biomarkers correlated with disease progression in clear cell renal cell carcinoma using desorption electrospray ionization imaging mass spectrometry. *Oncotarget* 10: 1688−1703, 2019.
9) Mamun M Al, Gonzalez TV, Islam A, Sato T, Sato S, et al: Analysis of potential anti-aging beverage Pru, a traditional Cuban refreshment, by desorption electrospray ionization-mass spectrometry and FTICR tandem mass spectrometry. *J Food Drug Anal* 27: 833−840, 2019.
10) Chi DH, Kahyo T, Islam A, Hasan MM, Waliullah A, et al: NAD^+levels are augmented in aortic tissue of ApoE-/- mice by dietary omega-3 fatty acids. *Arterioscler Thromb Vasc Biol* 42: 395−406, 2022.
11) Mamun A, Islam A, Eto F, Sato T, Kahyo T, et al: Mass spectrometry-based phospholipid imaging: Methods and findings. *Expert Rev Proteomics* 17: 843−854, 2021.
12) Lamont L, Eijkel GB, Jones EA, Flinders B, Ellis SR, et al: Targeted drug and metabolite imaging: Desorption electrospray ionization combined with triple quadrupole mass spectrometry. *Anal Chem* 90: 13229−13235, 2018.
13) Dannhorn A, Doria ML, McKenzie J, Inglese P, Swales JG, et al: Targeted desorption electrospray ionization mass spectrometry imaging for drug distribution, toxicity, and tissue classification studies. *Metabolites* 13: 377, 2023.
14) Formentini L, Moroni F, Chiarugi A: Detection and pharmacological modulation of nicotinamide mononucleotide (NMN) in vitro and in vivo. *Biochem Pharmacol* 77: 1612−1620, 2009.
15) Lee CF, Caudal A, Abell L, Nagana Gowda GA, Tian R: Targeting NAD^+metabolism as interventions for mitochondrial disease. *Sci. Rep.* 9: 3073, 2019.
16) Poljsak B: NAMPT-mediated NAD biosynthesis as the internal timing mechanism: In NAD^+world, time is running in its own way. *Rejuvenation Res* 21: 210−224, 2018.
17) Nadeeshani H, Li J, Ying T, Zhang B, Lu J: Nicotinamide mononucleotide (NMN) as an anti-aging health product—Promises and safety concerns. *J Adv Res* 37: 267−278, 2022.
18) Ito TK, Sato T, Takanashi Y, Tamannaa Z, Kitamoto T, et al: A single oral supplementation of nicotinamide within the daily tolerable upper level increases blood NAD^+levels in h,ealthy subjects. *Transl Med Aging* 5: 43−51, 2021.
19) Luo S, Zhao J, Zheng Y, Chen T, Wang Z: Biosynthesis of nicotinamide mononucleotide: Current metabolic engineering strategies, challenges, and prospects. *Fermentation* 9: 594, 2023.
20) Shen Q, Zhang SJ, Xue YZ, Peng F, Cheng DY, et al: Biological synthesis of nicotinamide mononucleotide. *Biotechnol Lett* 43: 2199−2208, 2021.
21) Ratcliffe NA, Mello CB, Garcia ES, Butt TM, Azambuja P: Insect natural products and processes: New treatments for human disease. *Insect Biochem Mol Biol* 41: 747−769, 2011.
22) Bartkiene E, Starkute V, Katuskevicius K, Laukyte N, Fomkinas M, et al: The contribution of edible cricket flour to quality parameters and sensory characteristics of wheat bread. *Food Sci Nutr* 10: 4319−4330, 2022.
23) Yan J, Sakamoto T, Islam A, Ping Y, Oyama S, et al: Cinnamomum verum J. presl bark contains high contents of nicotinamide mononucleotide. *Molecules* 27: 7054, 2022.
24) Bustamante S, Jayasena T, Richani D, Gilchrist RB, Wu LE, et al: Quantifying the cellular NAD^+metabolome using a tandem liquid chromatography mass spectrometry approach. *Metabolomics* 14: 15, 2017.
25) Paine MRL, Ellis SR, Maloney D, Heeren RMA, Verhaert PDEM: Digestion-free analysis of peptides from 30-year-old formalin-fixed, paraffin-embedded tissue by mass spectrometry imaging. *Anal Chem* 90: 9272−9280, 2018.
26) Siddiqui R, Elmashak Y, Khan NA: Cockroaches: A potential source of novel bioactive molecule(s) for the benefit of human health. *Appl Entomol Zool* 58: 1−11, 2023.
27) Mills KF, Yoshida S, Stein LR, Grozio A, Kubota S, et al: Long-term administration of nicotinamide mononucleotide mitigates age-associated physiological decline in mice. *Cell Metab* 24: 795, 2016.
28) Qu S, Kwon SJ, Duan S, Lim YJ, Eom SH: Isoflavone changes in immature and mature soybeans by thermal processing. *Molecules* 26: 24, 7471−7485, 2021.
29) Ma X, Hu Y, Li X, Zheng X, Wang Y, et al: Periplaneta americana ameliorates dextran sulfate sodium-induced ulcerative colitis in rats by Keap1/Nrf-2 activation, intestinal barrier function, and gut microbiota regulation. *Front Pharmacol* 9: 944, 2018.
30) Niaz K, Zaplatic E, Spoor J: diploptera functata (cockroach) milk as next superfood. *Excli J* 17: 721−723, 2018.
31) Donkor E S: Cockroaches and food-borne pathogens. *En-*

viron Health Insights 14: 1178630220913365, 2020.

32) Phesatcha B, Phesatcha K, Viennaxay B, Matra M, Totakul P, et al: Cricket meal (Gryllus bimaculatus) as a protein supplement on in vitro fermentation characteristics and methane mitigation. *Insects* 13: 129, 2022.

33) Ahn MY, Hwang JS, Yun EY, Kim MJ, Park KK: Anti-aging effect and gene expression profiling of aged rats treated with G. bimaculatus extract. *Toxicol Res* 31: 173, 2015.

34) Ishibashi T, Waliullah A, Aramaki S, Kamiya M, Kahyo T, et al: Plastic brain structure changes associated with the division of labor and aging in termites. *Dev Growth Differ* 65: 374−383, 2023.

35) Palermo V, Falcone C, Calvani M, Mazzoni C: Acetyl-L-carnitine protects yeast cells from apoptosis and aging and inhibits mitochondrial fission. *Aging Cell* 9: 570−579, 2010.

36) Tasaki E, Mitaka Y, Takahashi Y, Waliullah A., Tamannaa Z, et al: The royal food of termites shows king and queen specificity. *PNAS nexus* 2: 222, 2023.

Research Paper

Sex-specific effect of ethanol on colonic short-chain fatty acids and derivatives in the mouse model using targeted LC/MS

Siddabasave Gowda B. Gowda[1,2#*], Lipsa Rani Nath[1#], Yonghan Li[3], Jayashankar Jayaprakash[1], Divyavani Gowda[2], Shu-Ping Hui[2*]

[1]Graduate School of Global Food Resources, Hokkaido University, Kita-9, Nishi-9, Kita-Ku, Sapporo 060−0809, Japan
[2]Faculty of Health Sciences, Hokkaido University, Kita-12, Nishi-5, Kita-ku, Sapporo 060−0812, Japan
[3]Graduate School of Health Sciences, Hokkaido University, Kita-12, Nishi-5, Kita-ku, Sapporo 060−0812, Japan

Abstract Ethanol consumption affects the human body, particularly the digestive system, leading to gut dysbiosis and dysregulation of metabolites. Although previous studies have focused on the effects of ethanol on liver metabolism, colon-specific metabolites have not been well explored. In this study, we investigated the effects of ethanol on colon-specific short-chain fatty acids (SCFAs) and their derivatives in a mouse model using liquid chromatography-tandem mass spectrometry (LC-MS/MS). Colonic flush samples obtained from ethanol-fed (EF) and pair-fed (PF) mice of each sex were subjected to targeted analysis of SCFAs and SCFA esters of hydroxy fatty acids (SFAHFA) using LC-MS/MS. The levels of acetic acid (AA), propanoic acid (PA), and butyric acid (BA) were significantly increased in the male mouse EF group compared to those in the PF group. In contrast, the levels of AA and PA were decreased in female mice in the EF group compared to those in the PF group. Furthermore, the levels of AA-derived SFAHFAs were decreased in the male EF group but increased in the female EF group compared to those in the control group. Compared to the control groups, hydroxy fatty acid levels were significantly decreased in the EF groups of both sexes. Overall, ethanol exerted diverse effects on colon-specific metabolites in both male and female mice. This study provides new insights into sex-dependent metabolic changes associated with alcohol-induced gut microbiota dysfunction and their potential health impacts.

Key words: ethanol, short-chain fatty acids, SFAHFA, liquid chromatography, mass spectrometry, gut-microbial metabolites

1. Introduction

Alcohol is a globally prevalent psychoactive substance deeply rooted in various cultures that poses significant health risks. Alcohol was ranked as the seventh leading cause of death globally and contributed to 2.8 million deaths in 2016[1)]. The harmful effects of alcohol on the digestive system are closely related to the gut−liver axis, in which the enterohepatic circulation is essential for transporting products from the gut to the liver[2)]. Alcohol disrupts the gut−liver axis, altering the microbial composition and gut barrier integrity[3)], which leads to impaired nutrient absorption and contributes to conditions such as alcoholic hepatitis and cirrhosis. Dysbiosis disrupts tight junction proteins, allowing the translocation of particles into portal circulation[4)]. Tight junction maintenance is facilitated by short-chain fatty acids (SCFAs), which are byproducts of anaerobic fermentation by the food fibers[5)]. Fecal metabolome analysis of patients with alcohol use disorders showed a decrease in SCFAs, which could be explained by dysbiosis-impacting bacteria that produce SCFAs, including *Fae-*

#Equally contributing authors
*Corresponding author
[1]Siddabasave Gowda B. Gowda
Faculty of Health Sciences, Hokkaido University, Kita-12, Nishi-5, Kita-ku, Sapporo 060−0812, Japan
E-mail: gowda@gfr.hokudai.ac.jp
[2]Shu-Ping Hui
Faculty of Health Sciences, Hokkaido University, Kita-12, Nishi-5, Kita-ku, Sapporo 060−0812, Japan
Tel: +81−11−706−3693
E-mail: keino@hs.hokudai.ac.jp
Received: February 4, 2024. Accepted: February 28, 2024.
Epub April 16, 2024.
DOI: 10.24508/mms.2024.06.002

calibacterium[6].

Recent findings revealed a novel class of derivative lipids of SCFAs, namely SCFA esters of hydroxy fatty acids (SFAHFAs), which are abundant in the gut[7]. Gut microbiota is significant in the formation of these lipids, which are present in the colon and cecum[8]. Understanding the effect of alcohol on colonic-specific SCFAs and their derivatives was significantly advanced when chemically generated SFAHFAs were measured in rat intestinal contents and fecal samples[9].

Although existing research has explored lipid metabolism in alcohol-induced gut dysbiosis, notable gaps exist in our understanding of how ethanol specifically affects colonic SCFAs and SFAHFAs. A previous study used gas chromatography−mass spectrometry (MS) for analyzing human stool samples and demonstrated that excessive alcohol consumption disrupts the intestinal microbiota and causes dysbiosis, thus highlighting importance of fatty acids (FAs) in intestinal health and linking microbiota dysfunction to alcohol-related pathologies[10]. Furthermore, using liquid chromatography coupled with triple quadrupole and quadrupole time-of-flight MS, previous studies revealed that ethanol alters lipid metabolism by influencing the gut microbiota[11,12].

However, the existing literature on lipid metabolism in ethanol-induced gut dysbiosis is limited, and the sex-specific effects of ethanol on gut lipid metabolism remain unclear. Therefore, using liquid chromatography-tandem MS (LC-MS/MS), we investigated the sex-specific effects of ethanol on gut lipid metabolism in a mouse model. Unveiling the intricate connections between alcohol consumption and SCFA/SFAHFA variations, our findings contribute to a nuanced understanding of the mechanisms, offering the potential for sex-specific therapeutic strategies against alcohol-related pathologies.

2. Materials and Methods

2.1. Materials

LC/MS-grade solvents acetonitrile, methanol, and isopropanol, 1 M aqueous ammonium acetate, and acetic acid (AA) were purchased from Wako Pure Chemical Industries, Ltd. (Osaka, Japan). The reagents triethylamine (TEA), N,N-Dimethylethylenediamine (DMED), and acetic acid-d4 (AA-d4) and HPLC-grade chloroform were acquired from Sigma-Aldrich (St. Louis, MO, USA). Pentanoic acid-d9 (PA-d9) and palmitic acid-d31 were obtained from Cayman Chemical (Ann Arbor, MI, USA). Solid-phase extraction cartridges (MonoSpin C18-AX) were provided by GL Science (Tokyo, Japan). 2-Chloro-1-methylpyridinium iodide (CMPI), along with propionic acid (PA), butyric acid (BA), valeric acid (VA), and caproic acid (CA), were sourced from Tokyo Chemical Industry Co., Ltd. (Tokyo, Japan). The SFAHFA standards were synthesized in-house as per the protocols described in our previous study[9].

2.2. Animal samples

Male and female C57BL6 mice (8−10 weeks old) were bred at the institutional core facility after obtaining approval from The Institutional Animal Care and Use Committee at the University of Tennessee Health Science Center. Bothe male and female mice were fed a Lieber−DiCarli liquid diet (D710260, Dyets Inc., Bethlehem, PA, USA) for four weeks with ethanol (0% for two days, 1% for two days, 2% for two days, 4% for one week, 5% for one week, and 6% for one week) or pair-fed (PF) isocaloric maltodextrin (BioServ, Flemington, NJ, USA). At the end of the four-week feeding period, both groups of mice were euthanized, and the colonic contents were flushed with 3 mL of 0.9% saline. Flushed samples were frozen until lipid analysis. All experiments were performed in compliance with the relevant laws and/or institutional guidelines.

2.3. Extraction and targeted analysis of SCFA by LC-MS/MS

The extraction and analysis of SCFA were performed using the method developed in our previous studies[13]. Initially, 80 μL of acetonitrile was added to 20 μL of colonic flush, followed by the addition of 100 μL of 20 μM AA-d4 and 100 μL of 20 μM VA-d9 as internal standards. The mixture was then vortexed for 3 min at 3500 rpm and then centrifuged for 10 min at 15000 rpm and 4°C. The supernatant was carefully transferred into a new microtube, and derivatization was initiated by adding 20 μL of TEA and 10 μL of CMPI of 2 mM each. The mixture was vortexed for 3 min at 3500 rpm, following which 20 μL of 2 mM DMED was added to the microtube; the sample was further vortexed for 30 min at 3500 rpm and centrifuged (10 min, 15000 rpm, 4° C). The centrifugate was transferred to an LC vial, and 5 μL of this solution was injected into the LC-MS system.

Targeted analysis was performed using a Prominence ultrafast liquid chromatography (UFLC; Shimadzu, Kyoto, Japan) connected to a TSQ Quantum Mass Spectrometer

System (Thermo Fisher Scientific Inc., San Jose, CA, USA) operated in the positive-ion mode. The chromatographic separation was performed on a Hypersil GOLD C8 column (50 mm × 2.1 mm), which is a reversed-phase-type column with particle and pore sizes of 1.9 μm and 175 Å, respectively. The column oven was maintained at 40°C throughout the analysis. The mobile phase comprised a dual-solvent system: solvent A was Milli-Q water containing 20 mM ammonium acetate, and solvent B was a mixture of methanol and acetonitrile (50:50, v/v). The flow rate was set to 0.3 mL/min. The gradient program was initiated with solvent B at 100% for the first 1.5 min and held constant for 2 min. At 2.1 min, the proportion of solvent B was adjusted to 50% and maintained for 7 min. Subsequently, solvent B was returned to 100% after 7.5 min and maintained for 10 min. The electrospray ionization (ESI) source parameters were as follows: the spray voltage was 3,500 V; the sheath gas was 40 arbitrary units; the auxiliary gas was 25 arbitrary units; the capillary temperature was 250°C; and the HESI vaporizer temperature was 150°C. The SCFA concentrations were calculated from the linearity curves constructed using Xcalibur 2.2 software (Thermo Fisher Scientific., San Jose, CA, USA).

2.4. *Extraction and targeted analysis of SFAHFAs by LC-MS/MS*

The extraction and analysis of SFAHFAs were performed using a method developed in our previous studies[9]. Approximately 50 μL of colonic flush from ethanol-fed (EF) mice samples were transferred to Eppendorf tubes. To this, 100 μL of an internal standard mixture in methanol was added, which comprised 5 μM deuterated SFAHFA standard mixture (PAHPA-d30, BAHPA-d30, VAHPA-d30, and HAHPA-d30). In addition, 50 μL of methanol and 400 μL of Milli-Q water were added to the mixture. The resulting mixture was vortexed (3500 rpm, 1 min) and centrifuged (15,000 rpm, 1 min, 4°C) to collect the supernatant for solid-phase extraction using the MonoSpin C18-AX cartridges. The detailed workflow for the solid-phase extraction for SFAHFAs is described in our previous study[9].

Lipidomic analysis was conducted using a TSQ Quantum Access MAX Triple Quadrupole Mass Spectrometer (Thermo Fisher Scientific, Waltham, MA, USA) coupled with the Prominence UFLC system (Shimadzu, Kyoto, Japan) operating under ESI in negative mode. The LC-MS conditions closely adhered to the methodology established in our previous research[9]. The elution solvents consisted of 10 mM ammonium acetate (pump A), isopropanol (pump B), and methanol (pump C). An Atlantis T3 C18 column (50 mm × 2.1 mm, 3 μm, Waters, Milford, USA) was used for the chromatographic separation, which was maintained at 40°C with a flow rate of 300 μL/min. The elution gradient was set as follows: 40% B and 20% C (0−7 min), 80% B and 10% C (7−14 min), 30% B and 35% C (14−18 min), and returned to the initial conditions. For each injection, the sample volume was set to 10 μL.

2.5. *Statistical analysis*

Data were visualized using Microsoft Excel 2021 and GraphPad Prism version 8.0.1. Statistical analysis involved Student's t-test with $p<0.05$, which was considered significant.

3. Results

Fig. 1 shows the outcomes of SCFA analysis of the colon contents of EF and PF mice. The concentration of each acquired SCFA level is shown in the bar graphs. Male PF and EF mice exhibited lower SCFA levels than female mice. In particular, AA and PA levels significantly decreased in the EF group of females, whereas the trend was reversed in males. Conversely, BA and VA levels increased in male and female mice in the EF group, respectively. However, no significant differences were observed in CA levels between sexes.

The concentrations of SFAHFAs detected in colonic flush samples are shown in Fig. 2 (A−C). The overall SFAHFA concentrations were higher in males than in females. In particular, the levels of the AA ester of 2-hydroxy palmitic acid (2-AAHPA), AA ester of 2-hydroxy arachidic acid (2-AAHAA), AA ester of 2-hydroxy behenic acid (2-AAHBA), AA ester of 2-hydroxy tricosylic acid (2-AAHTA), AA ester of 2-hydroxy lignoceric acid (2-AAHLA), and AA ester of 2-hydroxy pentacosylic acid (2-AAHPSA) exhibited significant increases in the EF group of females compared to those in the PF group, whereas a reversed trend was observed in males. Furthermore, the AA ester of 2-hydroxy heneicosylic acid (2-AAHHA), BA ester of 2-hydroxy behenic acid (2-BAHBA), PA ester of 2-hydroxy cerotic acid (2-PAHCA), BA ester of 2-hydroxy cerotic acid (2-BAHCA), CA ester of 2-hydroxy cerotic acid (2-CAHCA), BA ester of 2-hydroxy lignoceric acid (2-BAHLA), and PA ester of 2-hydroxy pentacosylic acid

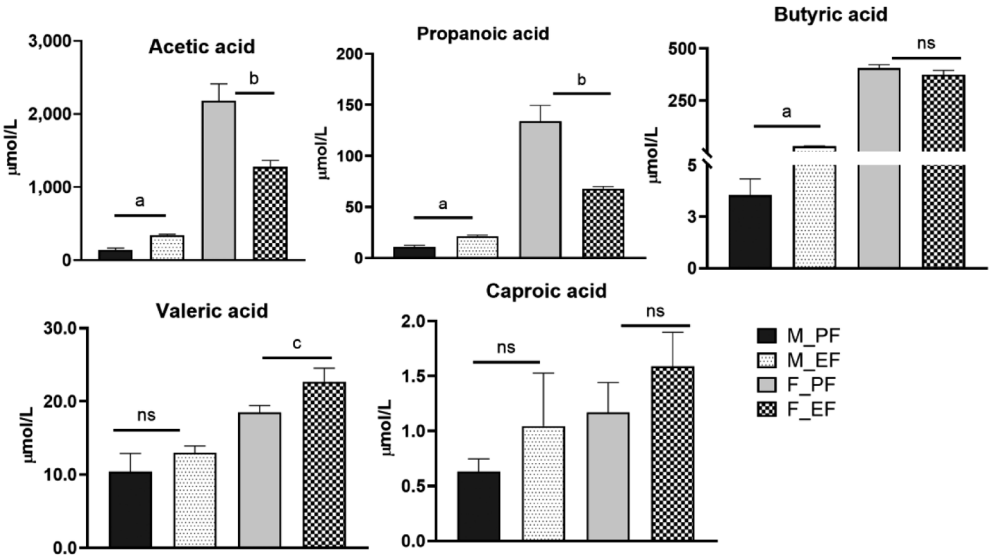

Fig. 1. Amount of SCFAs in colon contents of PF and EF groups of male and female mice.

(M_PF: Male pair-fed, M_EF: Male ethanol-fed, F_PF: female pair-fed, F_EF: female ethanol-fed, n=4 for each group). Student's t-test: $p<0.001$ (a), $p<0.01$ (b), $p<0.05$ (c), and ns: non-significant.

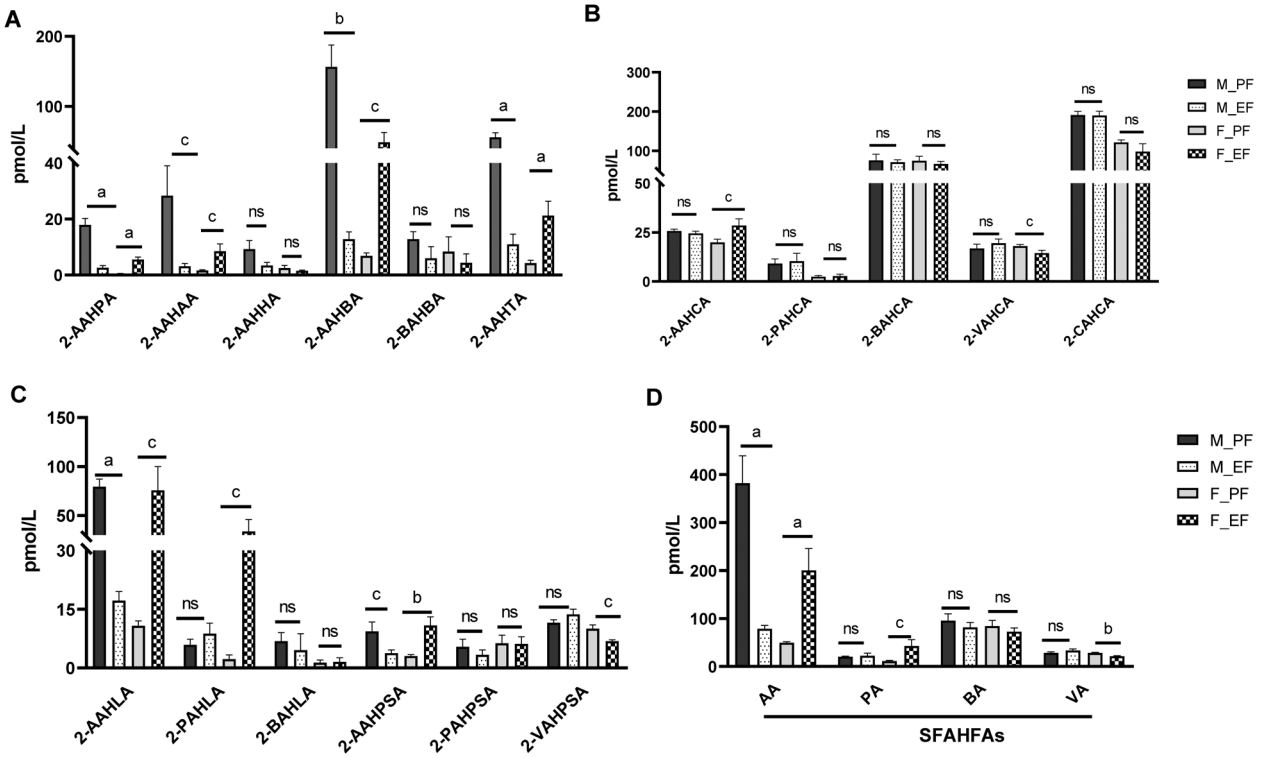

Fig. 2. Amount of SFAHFAs detected in colon contents of the PF and EF groups of male and female mice.

The concentrations of SFAHFAs at the molecular level are shown in A, B, and C, and the total SFAHFAs of each SCFA-derived lipids are shown in D. (M_PF: Male pair-fed, M_EF: Male ethanol-fed, F_PF: female pair-fed, F_EF: female ethanol-fed, n=4 for each group). Student's t-test: $p<0.001$ (a), $p<0.01$ (b), $p<0.05$ (c), and ns: non-significant.

(2-PAHPSA) did not show any significance between the EF and PF groups of sexes.

The levels of the AA ester of 2-hydroxy cerotic acid (2-AAHCA) and PA ester 2-hydroxy lignoceric acid (2-PAHLA) were significantly increased in female EF mice whereas no such differences were observed in male EF mice. However, the levels of the VA ester of 2-hydroxy cerotic acid (2-VAHCA) and VA ester of 2-hydroxy pentacosylic acid (2-VAHPSA) were significantly decreased in female EF mice, but no significant difference was observed

in male mice. Fig. 2(D) shows the total amount of SFAHFAs based on their SCFA acyl chains in the PF and EF mice of both sexes. In female mice, the levels of AA-derived SFAHFAs were significantly increased in the EF group, whereas the opposite trend was observed for the male mice. However, BA showed no significant differences between sexes. The levels of PA-derived SFAHFAs were significantly increased in the female EF group, whereas those of VA-derived SFAHFAs decreased. The concentrations of hydroxy FAs (HFAs) in PF and EF mice of both sexes are shown in Fig. 3. Notably, higher concentrations of HFAs were observed for females than males except for 2-hydroxy palmitic acid (2-HPA) in both the PF and EF groups. A significant decrease in HFA concentration was observed in female mice with EF. However, no significant variations were observed for HFA concentrations in male EF mice, except for 2-HPA and 2-hydroxy behenic acid (2-HBA), which were significantly decreased in the EF group. The concentrations of all the SCFA, SFAHFA, and HFA analyzed in the colonic flush samples of PF and EF mice were provided in Table 1. The data shows a large deviation in the concentration levels among each animal, suggesting that additional experiments with a large animal number would be essential to draw any further conclusions.

4. Discussions

Alcohol-induced dysbiosis has a detrimental effect on gut integrity, leading to the development of acute (alcoholic hepatitis) and chronic (alcohol-related cirrhosis) liver disorders. Many metabolites such as SCFAs are produced by the anaerobic gut microbiota as byproducts of the fermentation of dietary fibers[14,15] and have been demonstrated to have multiple favorable effects on mammalian energy metabolism[16]. Therefore, metabolites (such as SCFAs) produced by beneficial bacteria in the gut aid absorption and utilization. These metabolites also support mucosal immunity, preserve intestinal homeostasis, and shield the intestinal mucosal barrier.

As shown in Fig. 1, a significant decrease in the SCFA concentration was observed for the female EF mice compared to female PF mice. The relevance of these findings is further supported by a study on the fecal metabolome in humans with alcohol use disorders. This independent study revealed a reduction in SCFA levels, which is consistent with our results. The observed decrease in SCFAs is likely attributable, in part, to dysbiosis, which negatively affects SCFA-producing bacteria, namely *Faecalibacterium*[6,10]. The observed increase in SCFA levels in male EF mice may be attributed to inherent sex-specific hormonal and physiological differences. This is in agreement with a recent study on Chinese bamboo rats, which showed significant differences in microbial composition and genetic/metabolic pathways between female and male rats despite shared captive and feeding conditions[17]. These sex-specific variations may contribute to unique responses to alcohol exposure, influencing SCFA levels. The congruence between our mouse model results and the insights from the bamboo rat study highlights a robust association between ethanol consumption, gut dysbiosis, and alterations in SCFA levels in a sex-specific manner. Furthermore, parallel findings across different species enhance our understanding of the intricate relationships between alcohol consumption, gut microbiota, and downstream physiological effects.

The modulation of SFAHFAs in the PF and EF groups of both sexes is detailed in Fig. 2. Previous investigations into SFAHFAs have indicated a decline in their levels in the

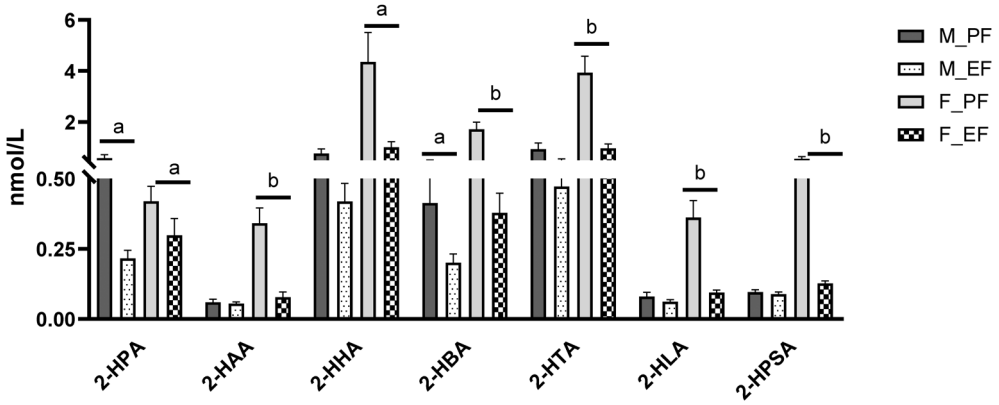

Fig. 3. Amount of hydroxy fatty acids detected in the PF and EF groups of male and female mice.
(M_PF: Male pair-fed, M_EF: Male ethanol-fed, F_PF: female pair-fed, F_EF: female ethanol-fed). Student's t-test: $p<0.001$ (a) and $p<0.01$ (b).

Table 1. The concentrations of short-chain fatty acids, SFAHFAs, and hydroxy fatty acids analyzed in the colonic flush samples

	Male mice								Female mice							
	PF1	PF2	PF3	PF4	EF1	EF2	EF3	EF4	PF1	PF2	PF3	PF4	EF1	EF2	EF3	EF4
SCFA	Concentration (μmol/L)															
Acetic acid	170.27	179.21	141.17	72.10	347.47	359.45	303.28	361.51	1938.33	1781.13	2181.98	2822.14	1205.66	1526.45	1266.54	1112.41
Propanoic acid	12.49	13.89	9.47	7.98	22.05	23.56	21.44	18.05	113.18	118.68	123.34	180.34	72.94	69.97	63.74	65.13
Butyric acid	4.52	4.27	4.21	1.15	28.96	35.08	26.96	32.18	381.42	375.36	428.11	440.38	388.65	410.53	384.06	309.70
Valeric acid	12.41	15.56	9.97	3.67	12.65	14.94	10.60	13.81	16.82	18.53	21.19	17.47	22.38	23.92	26.68	17.78
Caproic acid	0.32	0.83	0.59	0.78	1.24	0.28	2.33	0.33	0.51	1.48	0.95	1.73	1.87	1.75	2.05	0.68
SFAHFA	Concentration (pmol/L)															
2-AAHPA	13.14	16.03	18.49	24.00	0.78	4.00	3.62	1.99	0.87	0.00	0.00	0.56	3.94	5.77	7.77	4.59
2-AAHAA	9.86	13.74	33.51	56.24	4.31	0.59	4.91	2.68	1.90	1.20	0.87	2.33	3.69	4.58	10.88	14.77
2-AAHHA	4.69	3.27	14.75	14.28	5.58	2.59	0.62	4.80	2.48	3.41	0.00	4.09	0.93	2.16	1.08	1.81
2-AAHBA	82.97	125.93	206.27	210.27	18.07	5.62	12.66	14.81	4.11	8.23	6.56	8.57	31.37	18.15	70.79	74.44
2-BAHBA	14.76	19.52	8.33	8.45	0.00	0.00	6.20	17.58	23.43	7.32	0.00	2.62	2.39	13.73	0.00	1.29
2-AAHTA	53.74	40.22	56.92	71.75	8.25	3.45	11.69	20.53	5.33	6.45	1.70	3.43	19.71	7.34	29.85	28.01
2-AAHCA	24.07	24.41	27.96	26.50	23.91	21.59	25.06	27.32	17.04	17.26	22.09	23.29	26.82	38.15	27.33	21.54
2-PAHCA	4.93	15.74	8.32	7.66	4.33	22.30	8.36	6.18	1.74	1.76	4.32	1.80	3.10	0.00	4.94	2.89
2-BAHCA	59.86	40.31	94.74	108.01	77.16	56.25	83.23	67.73	67.42	78.72	47.28	104.35	76.47	78.12	50.83	60.93
2-VAHCA	11.10	15.50	20.02	20.39	20.21	20.60	23.68	13.51	17.03	16.63	18.31	20.12	18.54	14.51	13.28	11.31
2-CAHCA	200.01	190.97	207.92	165.63	200.45	208.75	191.88	158.62	135.42	112.72	109.77	128.03	109.25	150.49	68.24	63.15
2-AAHLA	86.57	58.90	75.62	95.98	20.05	13.44	22.17	13.00	11.16	13.41	11.19	7.28	36.32	30.99	115.21	119.97
2-PAHLA	9.73	4.99	2.63	6.17	13.49	13.10	3.13	5.24	0.50	5.43	2.12	0.94	31.76	7.71	66.58	28.26
2-BAHLA	8.80	1.34	5.80	11.45	0.00	0.88	17.23	0.00	1.37	0.00	3.27	0.69	0.00	0.00	4.29	1.95
2-AAHPSA	4.69	10.92	6.39	15.34	2.21	5.40	4.91	2.64	3.23	2.64	2.22	4.01	7.38	6.74	15.12	14.14
2-PAHPSA	7.44	0.54	9.40	4.28	2.17	2.28	7.06	1.90	12.05	6.17	4.45	2.55	3.13	4.61	5.24	11.52
2-VAHPSA	10.54	13.67	11.44	10.61	13.28	12.37	17.55	11.49	7.23	11.35	10.07	11.41	5.81	7.49	7.00	7.06
AA_SFAHFA	279.72	293.42	439.91	514.35	83.16	56.67	85.63	87.77	46.12	52.59	44.63	53.55	130.16	113.89	278.04	279.26
PA_SFAHFA	22.10	21.26	20.35	18.11	20.00	37.68	18.55	13.33	14.29	13.35	10.89	5.29	37.99	12.32	76.76	42.67
BA_SFAHFA	83.43	61.17	108.87	127.91	77.16	57.13	106.66	85.31	92.22	86.05	50.55	107.66	78.86	91.85	55.13	64.17
VA_SFAHFA	21.64	29.17	31.46	31.00	33.49	32.97	41.23	25.00	24.25	27.98	28.38	31.53	24.35	22.00	20.28	18.37
HFA	Concentration (nmol/L)															
2-HPA	0.48	0.40	0.48	0.98	0.23	0.15	0.20	0.28	0.29	0.49	0.52	0.38	0.21	0.18	0.41	0.39
2-HAA	0.07	0.04	0.04	0.08	0.07	0.04	0.05	0.06	0.20	0.41	0.44	0.31	0.06	0.04	0.10	0.12
2-HHA	0.74	0.58	0.50	1.27	0.60	0.30	0.36	0.42	1.90	6.79	5.78	2.95	0.66	0.59	1.39	1.38
2-HBA	0.43	0.30	0.23	0.69	0.28	0.13	0.19	0.20	1.04	2.13	2.19	1.50	0.31	0.21	0.47	0.51
2-HTA	0.96	0.66	0.54	1.60	0.68	0.28	0.44	0.49	2.33	4.87	5.11	3.41	0.80	0.58	1.20	1.29
2-HLA	0.08	0.06	0.05	0.12	0.08	0.05	0.05	0.07	0.21	0.45	0.47	0.32	0.09	0.07	0.11	0.11
2-HPSA	0.11	0.09	0.08	0.11	0.10	0.07	0.09	0.10	0.33	0.66	0.71	0.53	0.14	0.10	0.14	0.12

colons of rats subjected to a high-fat diet, in contrast to an increase observed in mice infected with the influenza virus[7,18]. The observed downregulation of specific SFAHFAs derived from PA and BA in antibiotic-treated mouse fecal samples underscores their specificity for the gut microbiota[12]. Previous studies have consistently demonstrated that supplementation with SCFAs, achieved through interventions such as a high-fiber diet or probiotics, enhanced gut epithelial integrity and mitigated liver injury in alcoholic models[19,20,21]. Considering the apparent association between SFAHFAs and SCFAs, these two biomolecules are reasonably correlated. This consistency strongly supports the continued exploration of interventions involving SCFAs and SFAHFAs as promising strategies for addressing pathologies associated with alcohol consumption.

A notable decrease in the HFA concentration in female EF mice is shown in Fig. 3. In male EF mice, except for 2-HPA and 2-HBA, no significant alterations were observed. As the generation of HFAs is linked with the abundance of free FAs (FFAs), these HFA results are in agreement with previous research that highlighted the pivotal role of FFA metabolism in the progression of alcoholic liver disease[22]. The implications of FFAs in alcohol-induced gut dysbiosis, characterized by microbiota imbalances and potential contribution to gastrointestinal disorders, have been accentuated in numerous studies[23]. An animal study has suggested that maintaining optimal intestinal FFA levels, particularly saturated fatty acids, can enhance and preserve the integrity of the intestinal gut barrier[24]. The observed decline in HFA concentration after ethanol consumption in our study adds to this understanding by emphasizing the intricate interplay between alcohol consumption, FA metabolism, and gut health. These findings reinforce the importance of targeted interventions to modulate HFAs, particularly in maintaining intestinal barrier integrity, as a potential strategy for addressing alcohol-related pathologies. The findings of the study are summarized

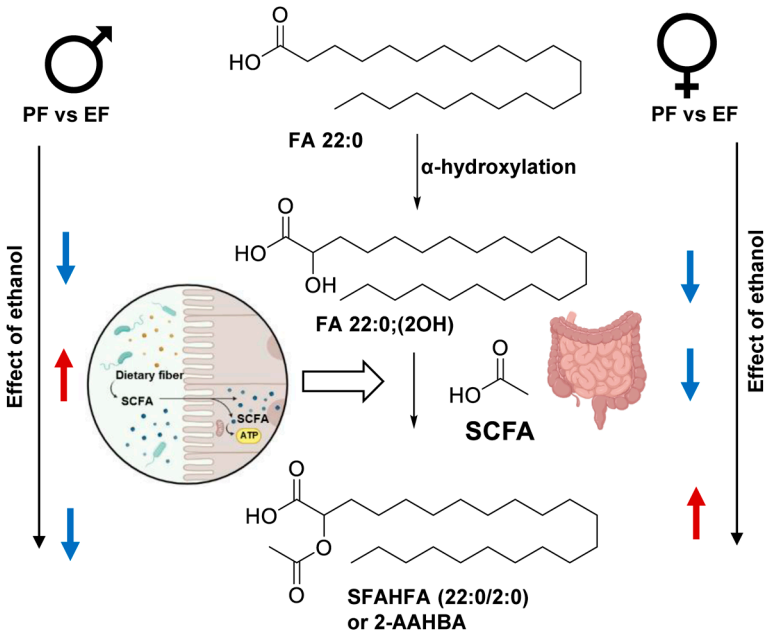

Fig. 4. Summary of changes in the precursor (FA 22:0(2OH), AA) and product (2-AAHBA) SFAHFA metabolism.

in Fig. 4 using a representative FA and its metabolites. The concentration of precursor FA 22:0(2OH) was decreased in the EF group of both sexes, and that of AA was increased in the male EF mice but decreased in female EF mice. However, an opposite trend was observed for 2-AAHBA in the EF groups of both sexes. This study has some limitations, including the mechanisms underlying the changes in the reported metabolites, which have not been explored. However, this study provides the first insight into the effects of ethanol on colonic metabolites produced by the gut microbiota.

In conclusion, our investigation into the effect of ethanol on colon-specific metabolites in a mouse model revealed distinct sex-dependent metabolic changes. These findings shed light on the intricate and diverse effects of alcohol-induced changes in gut microbiota, highlighting the importance of considering sex-specific responses to understand the potential health impacts of microbial metabolites.

Acknowledgements

We acknowledge the Japanese Society for the Promotion of Science (JSPS) KAKENHI grants: 19K0786109 to S-P Hui. 21K1481201 to S.G.B. Gowda and 22K1485002 to D. Gowda. We would like to deliver a special thanks to Dr. Pradeep K Shukla and Dr. Radhakrishna Rao for providing the animal samples. We would also like to acknowledge Editage, Japan for English proofreading of the manuscript and Graduate School of Global Food resources for covering English editing expenses.

Conflict of interest

The authors declare no competing financial interest.

References

1) Degenhardt L, Charlson, F, Ferrari, A, Santomauro, D, Erskine H, et al: The global burden of disease attributable to alcohol and drug use in 195 countries and territories, 1990−2016: A systematic analysis for the Global Burden of Disease Study 2016. *Lancet Psychiatr* 5(12): 987−1012, 2018.
2) Agustín A, De Gottardi A, Rescigno M: The gut-liver axis in liver disease: Pathophysiological basis for therapy. *Hepatol* 72(3): 558−577, 2020.
3) Kamran U, Towey J, Khanna A, Chauhan A, Rajoriya N, et al: Nutrition in alcohol-related liver disease: Physiopathology and management. *World J Gastroenterol* 26(22): 2916, 2020.
4) Stärkel P, Leclercq S, de Timary, P, Schnabl B: Intestinal dysbiosis and permeability: The yin and yang in alcohol dependence and alcoholic liver disease. *Clin Sci* 132(2): 199−212, 2018.
5) Ygor Parladore S, Bernardi A, Frozza. RL: The role of short-chain fatty acids from gut microbiota in gut−brain communication. *Front endocrinol* 11: 25, 2020.
6) Kamil L, Choroszy M, Waszczuk E: Changes in the composition of the human intestinal microbiome in alcohol

use disorder: A systematic review. *Am J Drug Alcohol Abuse* 46(1): 4−12, 2020.

7) Gowda SGB, Liang C, Gowda D, Hou F, Kawakami K, et al: Identification of short-chain fatty acid esters of hydroxy fatty acids (SFAHFAs) in a murine model by non-targeted analysis using ultra-high-performance liquid chromatography/linear ion trap quadrupole—Orbitrap mass spectrometry. *Rapid Commun Mass Spectrom* 34(17): e8831, 2020.
8) Gowda, SGB, Gowda D, Liang C, Li Y, Kawakami K, et al: Chemical labeling assisted detection and identification of short chain fatty acid esters of hydroxy fatty acid in rat colon and cecum contents. *Metabolites* 10(10): 398, 2020.
9) Gowda SGB, Hou F, Gowda D, Chiba H, Kawakami K, et al: Synthesis and quantification of short-chain fatty acid esters of hydroxy fatty acids in rat intestinal contents and fecal samples by LC-MS/MS. *Anal Chim Acta* 1288: 342145, 2024.
10) Couch RD, Dailey A, Zaidi F, Navarro K, Forsyth CB, et al: Alcohol induced alterations to the human fecal VOC metabolome. *PloS One* 10(3): e0119362, 2015.
11) Fang C, Zhou Q, Liu Q, Jia W, Xu Y: Crosstalk between gut microbiota and host lipid metabolism in a mouse model of alcoholic liver injury by chronic baijiu or ethanol feeding. *Food Funct* 13(2): 596−608, 2022.
12) Yasuda S, Okahashi N, Tsugawa H, Ogata Y, Ikeda K, et al: Elucidation of gut microbiota-associated lipids using LC-MS/MS and 16SrRNA sequence analyses. *iScience* 23 (12), 101841, 2020.
13) Gowda D, Li Y, Gowda, SGB, Ohno M, Chiba H, et al: Determination of short-chain fatty acids by *N*, *N*-dimethylethylenediamine derivatization combined with liquid chromatography/mass spectrometry and their implication in influenza virus infection. *Anal Bioanal Chem* 414(22): 6419−6430, 2022.
14) Douglas JM, T Preston: Formation of short chain fatty acids by the gut microbiota and their impact on human metabolism. *Gut Microbes* 7(3): 189−200, 2016.
15) Jian Kai T, Macia L, Mackay CR: Dietary fiber and SCFAs in the regulation of mucosal immunity. *J Allergy Clin Immunol* 151(2): 361−370, 2023.
16) Donohoe DR, Garge N, Zhang X, Sun W, O'Connell T M, et al: The microbiome and butyrate regulate energy metabolism and autophagy in the mammalian colon. *Cell Metab* 13(5): 517−526, 2011.
17) Gan Y, Wu YJ, Dong YQ, Li Q, Wu SG, et al: The study on the impact of sex on the structure of gut microbiota of bamboo rats in China. *Front Microbiol* 14: 1276620, 2023.
18) Gowda SGB. Gowda D, Ohno M, Liang C, Chiba H, et al: Detection and structural characterization of SFAHFA homologous series in mouse colon contents by LTQ-Orbitrap-MS and their implication in influenza virus infection. *J Am Soc for Mass Spectr* 32(8): 2196−2205, 2021.
19) Jiang XW, Li YT, Ye JZ, Lv LX, Yang LY, et al: New strain of Pediococcus pentosaceus alleviates ethanol-induced liver injury by modulating the gut microbiota and short-chain fatty acid metabolism. *World J Gastroenterol* 26(40): 6224, 2020.
20) Gail AC, Bush K, Nagy LE: Tributyrin supplementation protects mice from acute ethanol-induced gut injury. *Alcohol Clin and Exp Res* 38(6): 1489−1501, 2014.
21) Cresci GA, Glueck B, McMullen MR, Xin W, Allende D, et al: Prophylactic tributyrin treatment mitigates chronic-binge ethanol-induced intestinal barrier and liver injury. *Gastroenterol Hepatol* 32(9): 1587−1597, 2017.
22) Hwang S, Gao B: How does your fat affect your liver when you drink? *J Clin Invest* 129(6): 2181−2183, 2019.
23) Hartmann P, Seebauer CT, Schnabl B: Alcoholic liver disease: The gut microbiome and liver cross talk. *Alcohol Clin Exp Res* 39(5): 763−775, 2015.
24) Chen P, Torralba M, Tan J, Embree M, Zengler K, Stärkel P, et al: Supplementation of saturated long-chain fatty acids maintains intestinal eubiosis and reduces ethanol-induced liver injury in mice. *Gastroenterology* 148 (1): 203−214.e16, 2015.

Research Paper

Evaluation of four drug screening devices for detection of psychoactive drugs in pericardial fluid

Masae Iwai[1,2]*, Tadashi Ogawa[1,2], Tomohito Matsuo[1,2],
Katsutoshi Kubo[1,3], Fumio Kondo[1,4], Hiroshi Seno[1,2]

[1] Department of Legal Medicine, Aichi Medical University School of Medicine,
1−1 Yazakokarimata, Nagakute, Aichi 480−1195, Japan
[2] Poison Analysis Center, Aichi Medical University School of Medicine,
1−1 Yazakokarimata, Nagakute, Aichi 480−1195, Japan
[3] Department of Oral Pathology/Forensic Odontology, Aichi Gakuin University School of Dentistry,
1−100 Kusumoto-cho, Chikusa-ku, Nagoya, Aichi 464−8650, Japan
[4] Department of Biomedical Sciences, Chubu University College of Life and Health Sciences,
1200 Matsumoto-cho, Kasugai, Aichi 487−8501, Japan

Abstract We evaluated the applicability of four immunoassay-based drug screening devices, Triage® TOX Drug Screen, SIGNIFY™ ER, IVeX-screen M-1, and DRIVEN-FLOW M8-Z, in the detection of psychoactive drugs in pericardial fluid as an alternative to urine. A total of 38 pericardial fluid samples from forensic autopsies were analyzed with the four drug screening devices. To confirm the results, the concentrations of psychoactive drugs in pericardial fluid samples were measured together with those in urine and blood samples by liquid chromatography-tandem mass spectrometry. Only IVeX-screen M-1 precisely detected psychoactive drugs without false positive results, whereas Triage® TOX Drug Screen and SIGNIFY™ ER showed several false positive results, and DRIVEN-FLOW M8-Z led to many false positive results. These results suggest that IVeX-screen M-1 is more useful than other screening devices for psychoactive drugs in pericardial fluid and that pericardial fluid is a valid alternative material when urine is not available.

Key words: drug screening devices, psychoactive drugs, pericardial fluid, liquid chromatography-tandem mass spectrometry

Introduction

The detection of possible drug consumption is a central aspect of forensic toxicological examinations[1)]. Devices used for urine drug screening can provide a rapid indication of the presence of analytes of interest during autopsy[2)], but these devices are associated with several drawbacks. For example, Triage® DOA frequently returns false positive results in the detection of amphetamines[3−5)]. These false positive results are particularly important in the context of forensic autopsies, as they can be exacerbated by the production of putrefactive amines, such as 2-phenethylamine, by saprogenic bacteria in moderately or heavily decomposed bodies.

In our previous report, we evaluated the performance of five drug screening devices, Triage® TOX Drug Screen, SIGNIFY™ ER, IVeX-screen M-1, Status DS10, and DRIVEN-FLOW M8-Z, in the detection of amphetamines and methamphetamines in urine containing putrefactive amines. The results suggested that DRIVEN-FLOW M8-Z was more useful than other screening devices for screening of methamphetamines in the presence or absence of 2-phenethylamine, while none of the tested devices detected amphetamines precisely[6)].

Another issue with the forensic detection of drug use is

* **Corresponding author**
Masae Iwai
Department of Legal Medicine, Aichi Medical University School of Medicine, 1−1 Yazakokarimata, Nagakute, Aichi 480−1195, Japan
E-mail: masaoshi@aichi-med-u.ac.jp
Received: November 30, 2023. Accepted: March 31, 2024.
Epub May 20, 2024.
DOI: 10.24508/mms.2024.06.003

that collection of urine is not always feasible. In these cases, blood, pericardial fluid, cerebrospinal fluid, vitreous humor, or other alternative fluids must be analyzed. In particular, pericardial fluid often can be readily obtained from the pericardial cavity. Typical volumes of pericardial fluid taken at the time of autopsy range from 5 to 35 mL[7]; this amount is sufficient for forensic drug testing. Because of the potential utility of this material in forensic analyses, in the present study we evaluated the applicability of four drug screening devices, Triage® TOX Drug Screen, SIGNIFY™ ER, IVeX-screen M-1, and DRIVEN-FLOW M8-Z, to the detection of psychoactive drugs in pericardial fluid from autopsy samples. In this analysis, liquid chromatography-tandem mass spectrometry (LC-MS/MS) was employed as a sensitive and quantitative tool to compare the performance of these immunoassay-based devices.

Materials and Methods

Chemicals and materials

Amphetamine was kindly provided by Dr. Kenji Hara (Fukuoka University). The following standard drugs were used: methamphetamine (Dainihonseiyaku, Osaka, Japan); amobarbital (NIPPON SHINYAKU, Kyoto, Japan); bromazepam and flunitrazepam (Eisai, Tokyo, Japan); brotizolam (Sumitomo Pharma, Tokyo, Japan); estazolam (Takeda Pharmaceuticals, Tokyo, Japan); phenobarbital, amitriptyline, nortriptyline, diazepam and triazolam (Fujifilm Wako Pure Chemical, Osaka, Japan); temazepam, zolpidem, diazepam-d_5, and phenobarbital-d_5 (Sigma-Aldrich, St. Louis, MO, USA). High-performance liquid chromatography (HPLC)-grade methanol was obtained from Fujifilm Wako Pure Chemical (Osaka, Japan). Other common chemicals used were of the highest purity commercially available. Laboratory distilled water was purified using a Direct-Q UV 3 system (Millipore, Molsheim, France).

Biological samples

Pericardial fluid, urine and blood samples were obtained from autopsy cadavers at Aichi Medical University from 2021 to 2023. Samples were collected in 5- or 15-mL tubes and stored at −80°C until analysis. Additionally, pericardial fluid samples were assessed without any pretreatment.

Devices and their principles of detection

Triage® TOX Drug Screen (Alere San Diego, CA, USA), SIGNIFY™ ER (Innovacon, CA, USA), IVeX-screen M-1

Table 1. Cutoff values of psychoactive drugs for four drug screening devices

Drug classification	Drug name	Abbreviation*1	Cutoff values (ng/mL)			
			Triage® TOX Drug Screen	SIGNIFY™ ER	IVeX-screen M-1	DRIVEN-FLOW M8-Z
Barbiturates	Phenobarbital	BAR	230	100	150	2200
	Amobarbital	BAR	250	300	200	2000
Sedative-hypnotics	Bromazepam	BZO/BZD	750	1562	600	500
	Brotizolam	BZO/BZD	—*2	—*2	＞10000	—*2
	Estazolam	BZO/BZD	400	2500	400	—*2
	Flunitrazepam	BZO/BZD	200	390	400	—*2
	Lorazepam	BZO/BZD	200	1562	2000	550
	Midazolam	BZO/BZD	200	12500	10000	—*2
	Temazepam	BZO/BZD	200	98	—*2	—*2
	Triazolam	BZO/BZD	100	2500	600	300
	Zolpidem	ZOL	—*2	—*2	50	50
Tricyclic antidepressants	Amitriptyline	TCA	600	1500	300	1000
	Nortriptyline	TCA	900	1000	1000	1000
Stimulants	Amphetamine	AMP	500	1000	100000	85000
	Methamphetamine	mAMP/METH/MET	500	—*2	500	500

*1BAR; barbiturates, BZO/BZD; benzodiazepines, ZOL; zolpidem, TCA; tricyclic antidepressants, AMP; amphetamines, mAMP/METH/MET; methamphetamines.
*2Not available.

(Biodesign, Tokyo, Japan) and DRIVEN-FLOW M8-Z (Alfa Scientific Designs, CA, USA) were assessed in this study. All four devices are based on a competitive immunoassay and give qualitative responses to the presence or absence of drugs, and they are recommended to be used for urine only by their manufacturers. Cutoff values that are used by the devices to determine positive results are shown in Table 1.

LC-MS/MS analysis

Samples of human pericardial fluid, urine, or blood (100 μL) were mixed with 100 μL methanol and 200 μL acetonitrile after addition of 40 μL internal standard solution (0.5 μg/mL diazepam-d_5 and 25 μg/mL phenobarbital-d_5). The mixture was vortexed for 60 s and centrifuged at 15,000 g for 10 min, and the supernatant was transferred to another tube, followed by addition of 100 μL of 0.1% trifluoroacetic acid in acetonitrile. The solvent was removed with a centrifugal evaporator (CVE-200D; Tokyo Rikakikai, Tokyo, Japan). The residue was reconstituted in 100 μL methanol and centrifuged at 15,000 g for 1 min. A 5 μL aliquot of supernatant was subjected to analysis by LC-MS/MS. Samples containing high concentrations of target compounds were analyzed after dilution as needed.

LC-MS/MS analyses were performed using a Nexera X2 liquid chromatograph coupled to an LCMS-8040 mass spectrometer (Shimadzu, Kyoto, Japan). For separation, a Kinetex column (2.1 mm I.D. × 100 mm, particle size 2.6 μm; Phenomenex, Cheshire, UK) was used. The column temperature was maintained at 40°C. The gradient system used for separation included mobile phase A (a solution of 0.1% formic acid in 10 mM ammonium formate in water) and mobile phase B (a solution of 0.1% formic acid in 10 mM ammonium formate in methanol). The flow rate was 0.5 mL/min. The elution gradient involved a linear increase from 5% B to 95% B over 3.0 min, followed by constant 95% B for 1.5 min. The mobile phase was then returned to 5% B over 0.01 min and maintained at 5% B for 3.0 min to equilibrate the column for the next sample. The desolvation line temperature and heat block temperature were 250°C and 400°C, respectively.

Electrospray ionization was applied in the negative mode for phenobarbital and amobarbital and positive mode for other compounds. Quantification was performed by selected reaction monitoring (SRM) using the peak area. The SRM transitions were *m/z* 231→42 for phenobarbital, *m/z* 225→42 for amobarbital, *m/z* 136→91 for amphetamine, *m/z* 150→91 for methamphetamine, *m/z* 278→91 for amitriptyline, *m/z* 264→233 for nortriptyline, *m/z* 316→209 for bromazepam, *m/z* 393→314 for brotizolam, *m/z* 285→193 for diazepam, *m/z* 295→267 for estazolam, *m/z* 314→268 for flunitrazepam, *m/z* 301→255 for temazepam, *m/z* 343→308 for triazolam, *m/z* 308→235 for zolpidem, *m/z* 290→154 for diazepam-d_5 and *m/z* 236→42 for phenobarbital-d_5.

Ethics approval

All experiments were approved by the Ethics Committee of Aichi Medical University (approval no. 2020-172).

Results

A total of 38 pericardial fluid samples with matched urine and blood samples were obtained during forensic autopsies. The presence of psychoactive drugs was first evaluated in urine by Triage® TOX Drug Screen or SIGNIFY™ ER. Nine urine samples (cases 1–9) tested positive for the presence of at least one psychoactive drug (Table 2). The concentrations of the drugs in urine and blood samples were also determined by LC-MS/MS. The concentrations of drugs that were present in these samples were determined to be within the ranges of 2.0 to 20,300 ng/mL in urine samples (Table 2) and 0.50 to 3230 ng/mL in blood samples (Table 3). Because of low sample volumes, four urine and three blood samples were not analyzed by LC-MS/MS.

Pericardial fluid samples were then subjected to analysis with four drug screening devices: Triage® TOX Drug Screen, SIGNIFY™ ER, IVeX-screen M-1 and DRIVEN-FLOW M8-Z; these samples were also analyzed by LC-MS/MS. LC-MS/MS analysis revealed that 9 samples (cases 1, 2, 3, 6, 7, 8, 9, 11, 14 and 16) contained at least one type of psychoactive drug at a concentration between 9.8 and 3270 ng/mL (Table 4). A representative LC-MS/MS analysis of a pericardial fluid sample (case 7) shows peaks with the same retention times as those of standard amitriptyline (6.25 min) and nortriptyline (6.30 min) (Fig. 1a). Diagnostic fragment ions and their ion abundance ratios were also fully consistent with those of standard amitriptyline and nortriptyline, thus confirming the presence of these compounds in this pericardial fluid sample (Fig. 1b).

The results from the application of the four drug screening devices to pericardial fluid samples are summarized in Table 4. The Triage® TOX Drug Screen device returned

Table 2. Summary of results for drug screening devices and LC-MS/MS in urine samples

Case	drug screening device	Positive test result	LC-MS/MS (concentration, ng/mL)
1	Triage® TOX Drug Screen Drug Screen	mAMP, BZO, BAR	Phenobarbital (4630), Methamphetamine (1140), Amphetamine (247), Estazolam (37.3)
2	Triage® TOX Drug Screen	AMP, mAMP, BZO	Methamphetamine (1520), Amphetamine (317), Bromazepam (150),
3	SIGNIFY™ ER	BAR	Phenobarbital (6250)
4	Triage® TOX Drug Screen	mAMP, BZO	Methamphetamine (13260), Amphetamine (970), Temazepam (55.3), Diazepam (7.0)
5	Triage® TOX Drug Screen	BZO	Lorazepam (4.0)
6	Triage® TOX Drug Screen	BAR	Phenobarbital (1030)
7	Triage® TOX Drug Screen	BZO, TCA	Amitriptyline (513), Nortriptyline (200), Triazolam (1.2), Flunitrazepam (0.89)
8	Triage® TOX Drug Screen	BAR	Amobarbital (380)
9	Triage® TOX Drug Screen	AMP, mAMP, BZO	Methamphetamine (20300), Amphetamine (2680), Brotizolam (7.4), Flunitrazepam (5.2)
10	Triage® TOX Drug Screen	—	—
11	SIGNIFY™ ER	—	NT*
12	SIGNIFY™ ER	—	NT*
13	Triage® TOX Drug Screen	—	NT*
14	Triage® TOX Drug Screen	—	NT*
15	Triage® TOX Drug Screen	—	—
16	Triage® TOX Drug Screen		Zolpidem (0.20)
17–28	Triage® TOX Drug Screen or IVeX-screen M-1	—	—
29–38	Triage® TOX Drug Screen or SIGNIFYTM ER	—	—

*Not analyzed due to insufficient sample quantity.

Table 3. Quantification of psychoactive drugs in blood samples by LC-MS/MS

Case	Psychoactive drug (concentration, ng/mL)
1	Phenobarbital (3230), Estazolam (117), Methamphetamine (28.0), Amphetamine (5.1), Flunitrazepam (13.3)
2	Bromazepam (280), Methamphetamine (40.4), Nitrazepam (23.5), Amphetamine (17.5)
3	Phenobarbital (2610)
4	Methamphetamine (23.0), Temazepam (3.1), Amphetamine (3.0)
5	Lorazepam (3.7)
6	Phenobarbital (1750)
7	Amitriptyline (986), Nortriptyline (221), Flunitrazepam (6.9), Clonazepam (4.8), Triazolam (2.9)
8	Amobarbital (670)
9	Methamphetamine (190), Amphetamine (38.3), Flunitrazepam (19.1)
10	—
11	Midazolam (3.4)
12	NT*
13	NT*
14	NT*
15	—
16	Zolpidem (0.50)
17–28	—
29–38	—

*Not analyzed due to insufficient sample quantity.

Table 4. Summary of results for four drug screening devices and LC-MS/MS in pericardial fluid samples

Case	Triage® TOX Drug Screen	SIGNIFY™ ER	IVeX-screen M-1	DRIVEN-FLOW M8-Z	LC-MS/MS (concentration, ng/mL)
1	BAR	BAR	BAR	TCA*2, ZOL*2	Phenobarbital (744), Methamphetamine (7.0), Amphetamine (0.95) Estazolam (35.8)
2	—	BZO*3, TCA*2	—	TCA*2, ZOL*2	Bromazepam (24.1), Methamphetamine (8.9), Amphetamine (2.5)
3	BAR	BAR	BAR	BAR, ZOL*2	Phenobarbital (3270)
4	AMP*1	—	—	ZOL*2	Methamphetamine (6.3), Amphetamine (0.60)
5	—	—	—	ZOL*2	—
6	BAR	BAR	BAR	ZOL*2	Phenobarbital (505)
7	TCA*3	TCA*3	TCA	TCA*3	Amitriptyline (488), Nortriptyline (33.1)
8	BAR*3	—	BAR*3	ZOL*2	Amobarbital (116)
9	BZO*1	AMP*3	METH*3	MET	Methamphetamine (73.2), Amphetamine (9.8)
10		TCA*2	—	TCA*2, ZOL*2	—
11	BZO*3	—	—	ZOL*2	Midazolam (1.6)
12	—	TCA*2	—	TCA*2, ZOL*2	—
13	BZO*2	—	—	ZOL*2	—
14	BZO*3	—	—	TCA*2, ZOL*2	Midazolam (38.7)
15	*1	—	—	ZOL*2	—
16	—	—	—	ZOL*3	Zolpidem (0.928)
17–28	—		—	ZOL*2	—
29–38	—			TCA*2, ZOL*2	—

*1Undeterminable. *2False positive.
*3Positive even though the sample drug concentrations determined by LC-MS/MS analyses were under the cutoff values.

three ambiguous results (cases 4, 9 and 15) for unknown reasons, and it returned one false positive result for benzodiazepines (case 13). The SIGNIFY™ ER device produced three false positive results for tricyclic antidepressants. The IVeX-screen M-1 device returned no false positive results. The DRIVEN-FLOW M8-Z device returned false positive results for zolpidem or tricyclic antidepressants in 35 of the 38 cases.

Eleven samples (cases 2, 7, 8, 9, 11, 14 and 16) tested positive for psychoactive drugs according to drug screening devices, even though the sample drug concentrations determined by LC-MS/MS were under the immunoassay cutoff values that are considered to indicate positive results (Table 4). Therefore, to investigate this potential discrepancy, blank pericardial fluid samples spiked with psychoactive drugs at the concentrations found by LC-MS/MS analyses were subjected to analyses with the drug screening devices. Using a blank sample spiked with the concentration of TCA found in case 7 returned a positive result using Triage® TOX Drug Screen; the concentration of BZO from case 14 returned a positive result using Triage® TOX Drug Screen; and the concentration of ZOL from case 16 returned a positive result using DRIVEN-FLOW M8-Z. Other samples returned negative results for the spiked psychoactive drugs.

Discussion

In the present study, we investigated four drug testing devices with respect to their performance in detecting psychoactive drugs in forensic pericardial fluid samples. One of these devices, IVeX-screen M-1, was found to be more useful than the other three screening devices. This device accurately detected phenobarbital (cases 1, 3 and 6), amitriptyline (case 7), amobarbital (case 8) and methamphetamine (case 9), and returned no false positive results. On the contrary, the Triage® TOX Drug Screen and SIGNIFY™ ER devices returned several false positive results, and the DRIVEN-FLOW M8-Z device returned many false positive results. To our knowledge, the only information concerning the applicability of drug testing device to the detection of psychoactive drugs in pericardial fluid has been reported by Tominaga et al[5]. This report showed that Triage® TOX Drug Screen returned a few false positive results as ours and recommended the combined usage of another device to minimize misinterpretation prior to instru-

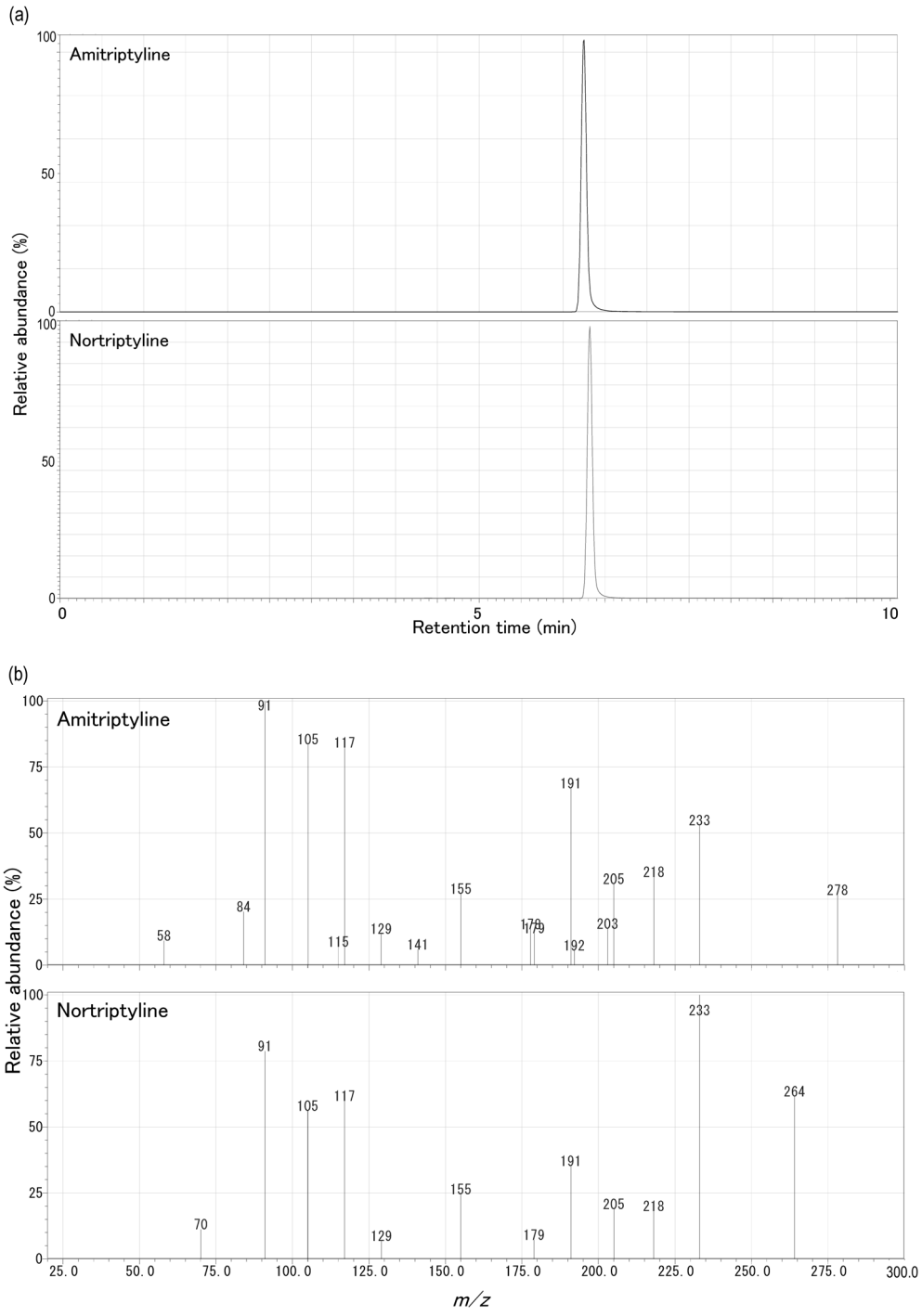

Fig. 1. Representative LC-MS/MS analysis of a pericardial fluid sample (case 7).

(a) Selective ion monitoring liquid chromatograms show the same retention times (6.25 min and 6.30 min) as those of standard amitriptyline and nortriptyline. (b) Diagnostic fragment ions with ion abundance ratios of the noted fractions from the pericardial fluid sample were fully consistent with those of standard amitriptyline and nortriptyline, thus confirming the presence of these compounds in this pericardial fluid sample.

mental analysis.

The principal advantage of the use of pericardial fluid is that pericardial fluid is easily obtained from the pericardial cavity, and the usual volume of pericardial fluid taken at the time of the autopsy is enough for forensic drug testing[7]. As the pericardial fluid is found in a closed compartment, contamination by microorganisms is less likely as compared to blood and cerebrospinal fluid, and pericardial fluid is thus relatively stable in the postmortem period[8]. In the present study, however, we found that drug concentrations were

lower in the pericardial fluid than in the urine. Specifically, the concentrations of methamphetamine and amphetamine in pericardial fluid were considerably lower than those in urine samples. We conclude, then, that pericardial fluid is an important alternative material when urine is not available, but it is unsuitable for detecting methamphetamine and amphetamine because of low concentrations compared to urine.

One of the disadvantage of immunoassays, including those investigated in the present study, is that antibodies tend to be variable in terms of their potentials for cross-reactivity[4]. This cross-reactivity can lead to inconsistent results or false positive signals. In our previous study, we found that the DRIVEN-FLOW M8-Z device was particularly useful for the detection of methamphetamines in forensic urine samples[6]. One advantage of this device when screening urine samples was the lack of false positive signals even in the presence of the putrefactive amine 2-phenethylamine. However, in the present study, this device led to many false positive results for zolpidem and tricyclic antidepressants. False positive results are relatively common with immunoassays, as antibodies tend to be variable in terms of their potentials for cross-reactivity. In this case, we hypothesize that antibodies employed by the DRIVEN-FLOW M8-Z device may cross-react with substances commonly found in the pericardial fluid, thus limiting its usefulness in this context.

We also investigated the potential discrepancy that eleven samples returned positive results for TCA, BZO and ZOL, even though the sample drug concentrations determined by LC-MS/MS were under the immunoassay cutoff values. As a result of test spiked with psychoactive drugs at the concentrations found by LC-MS/MS analyses, three samples returned positive results and other samples returned negative results. These discordant results remain unresolved, and further studies incorporating LC-MS/MS analyses will be performed to clarify the reasons for these discrepancies and to accurately evaluate the performance of the drug screening devices.

We used LC-MS/MS analyses to evaluate the results from the drug screening devices. LC-MS/MS has been widely used in recent bioanalytical work, since it is a powerful analytical technique that combines the resolving power of liquid chromatography with the detection specificity of mass spectrometry[9]. In the present study, we found that LC-MS/MS was more accurate and sensitive than were the immunoassay-based devices for the detection of psychoactive drugs. Thus, we recommend that positive results obtained using the screening devices should be confirmed by LC-MS/MS.

It should be noted that the concentrations of the drugs in the blood samples seem to be higher than those in the pericardial fluid, except for a couple of drugs such as phenobarbital in case 3. Because drug concentrations in pericardial fluid can be thought to be influenced from, or almost the same with those of blood from anatomical perspective, pericardial fluid thus has the potential to be very useful alternative when blood is not available.

In conclusion, pericardial fluid is an important alternative material for forensic analyses when urine is not available. Among the four drug screening devices tested for this application, we found IVeX-screen M-1 to be the most useful, as it accurately detected the highest number of psychoactive drugs without returning false positive results. Despite the accuracy of this device, it is strongly recommended LC-MS/MS methods should be used to confirm any positive results achieved with immunoassay-based screening devices.

Conflict of Interest

The authors declare no conflicts of interest.

References

1) Harper L, Powell J, Pijl EM: An overview of forensic drug testing methods and their suitability for harm reduction point-of-care services. *Harm Reduct J* 14: 52, 2017.
2) Towler S, Concheiro M, Pearring S, Rodda LN: Evaluation and applicability of Alere iCup DX 14 for rapid postmortem urine drug screening at autopsy. *J Forensic Sci* 66: 375−382, 2021.
3) Contreras MT, Hernández AF, González M, González S, Ventura R, et al: Application of pericardial fluid to the analysis of morphine (heroin) and cocaine in forensic toxicology. *Forensic Sci Int* 164: 168−171, 2006.
4) Maharjan AS, Johnson-Davis KL: Issues of interferences with immunoassays used for screening of drugs of abuse in urine, in Dasgupta A (ed): *Critical issues in alcohol and drugs of abuse testing*. p. 129, Elsevier, Amsterdam, 2019.
5) Tominaga M, Michiue T, Maeda H: Evaluation of the on-site immunoassay drug-screening device Triage-TOX in routine forensic autopsy. *Legal Med* 17: 499−502, 2015.

6) Iwai M, Ogawa T, Matsuo T, Kondo F, Kubo K, et al: Evaluation of five drug screening devices for testing of amphetamines and methamphetamines. *Med Mass Spectom* 6: 64−69, 2022.
7) Ferreira E, Corte Real F, Pinho E Melo T, Margalho C: A novel bioanalytical method for the determination of opioids in blood and pericardial fluid. *J Anal Toxicol* 44: 754−768, 2020.
8) Contreras MT, González M, González S, Ventura R, Valverde JL, et al: Validation of a procedure for the gas chromatography-mass spectrometry analysis of cocaine and metabolites in pericardial fluids. *J Anal Toxicol* 31: 75−80, 2007.
9) D'Ovidio C, Locatelli M, Perrucci M, Ciriolo L, Furton KG, et al: LC-MS/MS application in pharmacotoxicological field: current state and new applications. *Molecules* 28: 2127, 2023.

Research Paper

Plasma vitamin K-dependent protein C as early diagnostic marker of feline chronic kidney disease

Hiroto Maeda[1], Yuiko Suzuki[2], Kokoro Masuda[2], Yoshio Kodera[3], Toshifumi Watanabe[4], Kazuyuki Sogawa[2]

[1] Maeda Veterinary Hospital, 1−4−8 Yamatemachi, Tomakomai, Hokkaido 053−0851, Japan
[2] Department of Biochemistry, School of Life and Environmental Science, Azabu University, 1−17−71 Fuchinobe, chuo-ku, Sagamihara, Kanagawa 252−5201, Japan
[3] Center for Disease Proteomics, Kitasato University School of Science, 1−15−1 Kitasato, Minami-ku, Sagamihara, Kanagawa 252−0373, Japan
[4] DVMs Animal Medical Center Yokohama, 2−2 Sawatari, Kanagawa-ku, Yokohama, Kanagawa 221−0844, Japan

Abstract Chronic kidney disease (CKD) is a common disorder and cause of death in cats. In the classification proposed by the International Renal Interest Society (IRIS), stage 1 and 2 CKD are difficult to diagnose accurately using markers, in comparison with normal control cats. We recently described a simple and highly reproducible tandem mass tag (TMT) labelling method for identifying potential disease-marker candidates among low-abundance plasma proteins. In the current study, plasma samples were obtained from 90 normal control cats and 50 cats with CKD (stage 1). To identify new plasma biomarkers for CKD, six plasma samples (three from normal control cats and three from CKD stage 1 cats) were extracted with SSA lectin magnetic beads, differentially labelled with TMTs, digested with trypsin and subjected to analysis using LC-MS/MS. Sialylated Vitamin K-dependent protein C was identified as a protein with lower levels in CKD stage 1 cats compared to normal control cats. An ELISA of plasma sialylated vitamin K-dependent protein C showed within-run (4.3−4.9%) and between-day (4.3−5.2%) reproducibility. Plasma sialylated vitamin K-dependent protein C levels measured with this assay were significantly greater in normal control cats than in CKD stage 1 cats (1.40±0.13 vs. 1.07±0.11 AU/mL, $p < 0.001$). These results indicate that sialylated vitamin K-dependent protein C may be useful as a complementary marker with plasma creatinine, BUN and SDMA for detection of CKD stage 1 in cats.

Key words: chronic kidney disease, feline, plasma, vitamin K-dependent protein C

Introduction

Feline renal diseases are increasingly common in veterinary practice[1)]. It is important to diagnose and identify the pathological basis of renal dysfunction accurately at an early stage, since early diagnosis and treatment can delay progression of renal dysfunction, which leads to prolongation of survival and improvement of QOL[2)]. However, there are only a few reports on this area in clinical veterinary medicine[3)].

In daily clinical practice, plasma creatinine (p-Cre) and serum symmetric dimethylarginine (SDMA) are used as markers based on the stage classification criteria of the International Renal Interest Society (IRIS)[4)]. However, many of these markers have low specificity for renal function and there is a blind area without abnormal values, despite development of mild renal dysfunction. Therefore, it is especially important to evaluate the transitional period from a normal status to Stage 1 in the IRIS classification for early diagnosis of renal function. However, it is difficult to identify a mild decrease of renal function in the early phase using the available markers in clinical practice. In stage 1 there may not be any reduction in GFR or surrogate

* **Corresponding author**
Kazuyuki Sogawa
Department of Biochemistry, School of Life and Environmental Science, Azabu University, 1−17−71 Fuchinobe, Chuo-ku, Sagamihara, Kanagawa 252−5201, Japan
Tel: +81−42−769−1924, Fax: +81−42−769−1924
E-mail: sogawa@azabu-u.ac.jp
Received: February 6, 2024. Accepted: April 3, 2024.
Epub May 10, 2024.
DOI: 10.24508/mms.2024.06.004

markers of GFR, despite ongoing active disease in the kidney.

We recently described a simple and highly reproducible tandem mass tag (TMT) labelling method for identifying potential disease-marker candidates among low-abundance plasma proteins[8]. In this study, we used the lectin and tandem mass tag (TMT) method to generate comparative protein profiles of plasma samples from normal control cats and CKD stage 1 cats. Plasma levels of candidate proteins were compared to evaluate their potential to discriminate between the normal control cats and CKD cats. Novel plasma biomarkers were identified that may be superior to classical markers for early and specific detection of CKD stage 1 in cats.

Materials and Methods

Animals

Plasma samples from 50 cats with stage 1 CKD and 10 cats with stage 2 CKD brought to Maeda Veterinary Hospital between January 6, 2017 and February 20, 2018 (American Shorthair: 5, Chinchilla: 2, Mix: 53; 29 males and 31 females; age 2−13 years) were used in the study. Plasma samples from 90 cats aged 2−13 years (Scottish Fold: 4, American Shorthair: 2, Mix: 84; 43 males and 47 females) were used as normal control cats. Cats clinically diagnosed as normal based on serum biochemistry and ultrasonography tests were defined as normal cats, and cats showing clinical signs of CKD in blood chemistry were defined as those with stage 1 CKD. Criteria for normal urinalysis were urine specific gravity (USG) ＞1.030, urinary protein to creatinine ratio (UPC) ≤0.2, and a negative bacteriologic urine culture[5]. Diagnosis of CKD was made prior to inclusion in the study, based on clinical and laboratory findings. After stabilization, cats were classified[5] into 2 groups with p-Cre of ＜1.6 and 1.6−2.8 mg/dL in stages 1 and 2, based on the IRIS guidelines. Diagnosis of stage 1 CKD was made if p-Cre was ＜1.6 mg/dL, urine concentrating ability had been lost, other disorders related to decreased urine concentrating ability were excluded, and ultrasonographic changes were consistent with CKD (e.g., small kidney size and poor or absent renal corticomedullary differentiation)[6]. Samples were centrifuged at 1,710×*g* for 10 min (Model 6200; Kubota, Tokyo, Japan) and then stored at −80°C for further use. The ethics committee for Maeda Veterinary Hospital approved the protocol (2016-02). All owners gave signed informed consent to participation of their animal in the study.

Magnetic bead sample preparation using the Glycoprotein Isolation Kit

Paramagnetic non-porous particles coupled with a sambucus sieboldiana lectin ligand (MB-SSA; Bruker Daltonics, Bremen, Germany) were used to process the plasma samples. Binding, washing and elution solutions were prepared according to the manufacturer's instructions. MB-SSA binding solution (10 μL) and plasma (5 μL) were transferred to a 0.2− mL thin-walled tube. A homogenous magnetic-particle solution (10 μL) was added, mixed, and incubated for 5 min. The tubes were placed in an 8×12-well magnetic-bead separator (MBS; Bruker Daltonics) for 30 sec for magnetic fixation of the MB-SSA particles. The supernatant was aspirated and the tubes were removed from the MBS device. Washing solution (100 μL) was added and carefully mixed with the magnetic beads. The tube was placed back in the MBS device and moved back and forth sequentially between adjacent wells on each side of the magnetic bar of the device. After fixation of the magnetic beads for 30 s, the supernatant was aspirated. This washing procedure was repeated three times. After the final washing step, the bound molecules were eluted by incubation with 10 μL MB-SSA elution solution for 1 min, before the eluate was collected using the MBS device.

Tandem mass tag (TMT) labelling

Reduction and alkylation were performed as described previously[7]. A TMT sixplex Isobaric Label Reagent Set (Thermo Scientific, Rockford, IL, USA) was used according to the manufacturer's instructions. Tubes containing the different isobaric chemical tags (0.8 mg each) were added to 41 μL of anhydrous acetonitrile and dissolved for 5 min with occasional vortexing at room temperature. TMT solution (20 μL) was added to each tube and allowed to react at room temperature for 60 min. A volume of 4 μL of 5% hydroxylamine was added to each sample and the mixture was incubated for 15 min to quench the reaction[7]. Samples were finally pooled and lyophilized. Analyses were performed for samples of 20 μL of glycoprotein-isolated plasma from normal control cats (n=3) (TMT6-126, 127 and 128) and stage 1 CKD cats (n=3) (TMT6-129, 130 and 131). Plasma samples were randomly drawn.

Protein identification and quantification by LC-MS/MS analysis

Trypsin-digested peptides were injected into a trap col-

umn (C18, 5μm, 0.3×5mm) (IonPac; Thermo Scientific, Rockford, IL, USA) and an analytical column (C18, 3 μm, 0.075×120mm) (C18 packed emitter column；Nikkyo Technos, Tokyo, Japan) attached to an HPLC system (Ultimate 3000; Thermo Scientific). The flow rate of the mobile phase was 300nL/min. The solvent composition of the mobile phase was programmed to change in 120min cycles, with varying mixing ratios of solvent A (2% acetonitrile and 0.1% formic acid) to solvent B (90% acetonitrile and 0.1% formic acid), as described previously[7]. Purified peptides from HPLC were moved to a hybrid ion-trap Fourier transform mass spectrometer (LTQ-Orbitrap XL; Thermo Scientific) and analyzed using previously established parameters[8]. A database search engine (Proteome Discoverer; Thermo Scientific) was used to identify and quantify proteins from the mass, tandem mass and reporter ion spectra of peptides. Peptide mass data were matched by searching the UniProt database (https://www.uniprot.org/proteomes/?query=*) using the search parameters: peptide mass tolerance=2ppm and fragment tolerance=0.6Da, with the enzyme parameter set to trypsin, allowing up to one missed cleavage variable modification, methionine oxidation, and cysteine alkylation. The minimum criteria for protein identification were filtered with Xcorr vs. charge state and a false discovery rate (FDR) ＜1%.

ELISA

Immunization and establishment of hybridoma cell lines

Synthetic peptides of 20 amino acids (vitamin K-dependent protein C N peptide; FUJIFILM, Osaka, Japan) were used for immunization of BALB/c mice. Hybridoma cell line vitamin K-dependent protein C N-01[9] was established and antibody isotypes were determined using a Mouse Monoclonal Antibody Isotyping Test Kit (AbD Serotec, Kidlington, United Kingdom). To obtain pure monoclonal antibodies on a large scale, BALB/c mice were initially stimulated with 1.0mL pristine (Sigma-Aldrich, St. Louis, MO, USA) and then inoculated 2 weeks later. Monoclonal antibodies were purified as described elsewhere[9].

Immobilization of antibodies on a polystyrene microtiter plate

The anti-vitamin K-dependent protein C N peptide antibody dissolved in PBS buffer was dispensed into a 96-well polystyrene microtiter plate (Thermo Scientific, Rockford, IL, USA) at 0.5mg/well and incubated for 1 day at 4˚C. The plate was washed three times with PBS containing 0.05% Tween-20 (PBST). The microtiter plate was coated with 20% NOF102 containing 10% sucrose for 1 day at 4˚C.

ELISA conditions

After washing the microtiter plate with PBST, 100-μL aliquots of 10-times diluted plasma samples were added in duplicate to wells. The plates were incubated at room temperature for 1h and then washed three times. HRP-conjugated SSA lectin (Vector Laboratories, Burlingame, CA, USA) in PBST (100μL) was added to each well and the plate was incubated at room temperature for 30min. The plate was washed three times and then 100μL of TMB solution (FUJIFILM, Osaka, Japan) was added. After incubation at room temperature for 10min, 100μL of stop solution was added and the absorbance at 450nm was measured.

Other procedures

Creatinine was measured enzymatically with creatinine deiminase using a Fuji DRI-CHEM Slide CRE-PIII kit (FUJIFILM, Osaka, Japan). Blood urea nitrogen (BUN) was measured using a N-Assay BUN-L Nittobo D-Type kit (Nittobo Medical, Tokyo, Japan). Plasma SDMA was measured using a Cat SDMA ELISA Kit (MyBioSource, San Diego, CA, USA). Serum levels of vitamin K-dependent protein C was determined by enzyme-linked immunosorbent assays according to the manufacturer's instructions (ELISA Kits for vitamin K-dependent protein C, LifeSpan Biosciences. Seattle, WA, USA).

Statistical analysis

Statistical analysis was performed using IBM SPSS Statistics 19 (SPSS, Chicago, IL, USA). Numerical data are presented as the mean±standard deviation (SD). Differences in non-parametric data between two groups were analyzed by Mann-Whitney U-test, three groups were analyzed by Steel-Dwas test, with $P<0.05$ considered significant. Receiver operating characteristic (ROC) curves were constructed to assess the sensitivity, specificity, and areas under the ROC curves (AUCs).

Results

Identification of candidate proteins as markers of CKD stage 1

Clinical characteristics and biochemical variables of the

normal control cats and CKD groups are shown in Table 1. To identify new plasma biomarkers for CKD, six plasma samples (three normal control cat and three CKD stage 1) were alkylated with iodoacetamide, digested with trypsin, differentially labelled with TMTs, pooled and subjected to analysis using LC-MS/MS (Fig. 1). The three normal control cat samples were labelled with TMTs with reporter ions at *m/z*=126, 127 and 128, and the three CKD stage 1 samples were labelled with TMTs with reporter-ions at *m/z*= 129, 130 and 131. After comparing the profiles of proteins by LC-MS/MS using an LTQ Orbitrap XL mass spectrometer, 18 sialylated glycoproteins with unique peptide sequences were found with higher levels in normal control cats compared to CKD stage 1 cats (Table 2). Among these proteins, hemoglobin subunit alpha and vitamin K-dependent protein C had plasma levels elevated more than two-fold in all three normal control cats compared to the CKD stage 1 cats. Vitamin K-dependent protein C was selected for further analysis.

Establishment of an ELISA for sialylated vitamin K-dependent protein C

Range, dilution analysis and detection limit

A standard curve was drawn based on the colorimetric intensity of diluted recombinant cat vitamin K-dependent protein C (Cusabio Technology) to establish the relationship of intensity with the sialylated vitamin K-dependent protein C concentration (Fig. 2). The assay had a working range of 0−10AU/mL and gave linear results from 0 to 10AU/mL ($y=0.021\times-0.0018$, $r^2=0.9993$, $p<0.0001$). The detection limit was estimated by assaying the zero concentration eight times, and was defined as the sialylated vitamin K-dependent protein C "zero" concentration+3SD. The limit was found to be 0.18AU/mL.

Within-run and between-run reproducibility

The precision of the assay was determined using two sialylated vitamin K-dependent protein C concentrations of 0.5 and 2.0AU/mL. Within-assay CVs were determined with eight replicates of each sample. Between-assay CVs

Table 1. Clinical characteristics and biochemical variables of normal control cats and CKD cats

Variables	Normal control cats	CKD group		p-Value
		Stage 1	Stage 2	
Age (Mean±s.d.)	6.8±3.6	6.7±3.3	6.8±3.6	0.825
Sex (male, female)	90 (43, 47)	50 (24, 26)	10 (5, 5)	0.793
Blood urea nitrogen (mg/dL) (Mean±s.d.)	24.1±5.7	25.6±6.8	26.8±5.9	0.714
p-Creatinine (mg/dL) (Mean±s.d.)	0.96±0.23	1.20±0.23	1.99±0.24	0.015
Symmetric dimethylarginine (mg/dL) (Mean±s.d.)	5.9±0.8	6.4±1.0	10.9±1.6	0.009
Urine specific gravity (Mean±s.d.)	1.053±0.006	1.051±0.005	1.045±0.016	0.618
Urinary protein to creatinine ratio (Mean±s.d.)	0.13±0.04	0.15±0.05	0.17±0.06	0.024

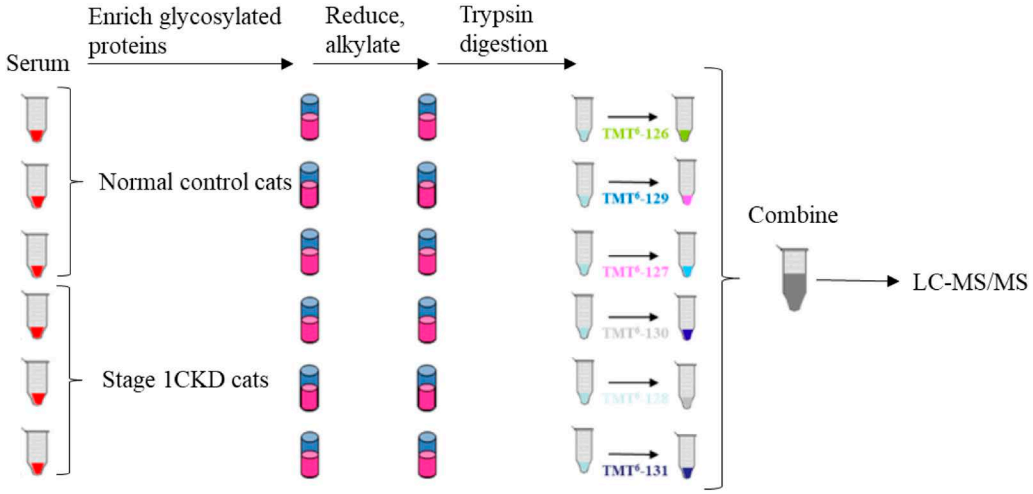

Fig. 1. Identification of candidate proteins using TMT labelling and LC-MS/MS analyses.

Table 2. Plasma sialylated glycoproteins detected at higher levels in normal control cats compared to CKD stage 1 cats in proteome analysis

Database Accession No.	ID	Coverage (%)	Number of matching peptides	TMT							
				Normal control cats				Stage 1 CKD cats			
				126	127	128	Average	129	130	131	Average
M3W3E7	Alpha-2-macroglobulin	3.46	6	0.268	0.233	0.226	0.242	0.206	0.134	0.152	0.164
M3WPG6	Apolipoprotein A-I	12.41	4	0.298	0.240	0.167	0.235	0.236	0.108	0.139	0.161
M3WG78	ATP synthase subunit beta	8.00	3	0.212	0.158	0.133	0.168	0.277	0.106	0.113	0.166
M3W7M4	Attractin	4.69	6	0.260	0.134	0.307	0.234	0.180	0.164	0.133	0.159
M3WB05	Bifunctional purine biosynthesis protein ATIC	2.86	2	0.357	0.164	0.154	0.225	0.282	0.122	0.121	0.175
M3VZY7	Ceruloplasmin	5.63	4	0.230	0.142	0.268	0.213	0.230	0.136	0.142	0.169
M3WKP2	Clusterin	16.63	13	0.391	0.132	0.263	0.262	0.140	0.157	0.140	0.146
M3VU42	Complement factor I	2.31	2	0.394	0.162	0.227	0.261	0.106	0.263	0.219	0.196
P14450	Fibrinogen alpha chain (Fragment)	100	1	0.191	0.191	0.245	0.209	0.198	0.160	0.175	0.178
P14469	Fibrinogen beta chain	5.43	3	0.217	0.237	0.251	0.235	0.270	0.214	0.156	0.213
M3WB06	Fibronectin	4.24	8	0.194	0.155	0.270	0.207	0.297	0.181	0.131	0.203
P07405	Hemoglobin subunit alpha	18.44	2	0.480	0.336	0.198	0.338	0.167	0.130	0.133	0.143
M3WEG4	Phosphatidylinositol-glycan-specific phospholipase D	3.93	3	0.487	0.114	0.220	0.274	0.122	0.130	0.224	0.159
P49064	Serum albumin	31.58	19	0.251	0.177	0.130	0.186	0.278	0.131	0.128	0.179
M3WEV9	Transthyretin	8.84	2	0.169	0.121	0.188	0.159	0.118	0.189	0.116	0.141
M3WFT7	UDP-glucose 4-epimerase	2.66	2	0.152	0.208	0.217	0.192	0.251	0.174	0.099	0.174
Q28412	Vitamin K-dependent protein C	14.21	3	0.280	0.291	0.289	0.287	0.132	0.140	0.137	0.136
M3W9I5	Vitronectin	5.47	2	0.337	0.343	0.388	0.356	0.236	0.197	0.186	0.206

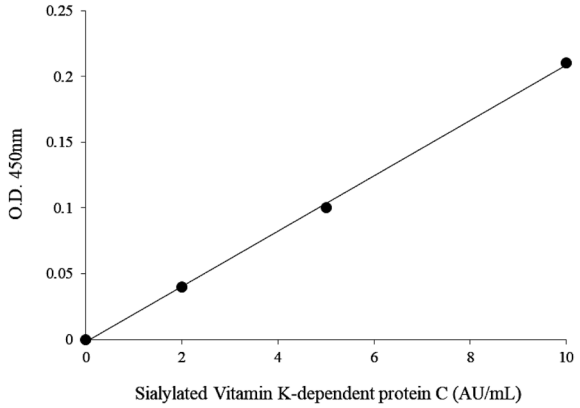

Fig. 2. Standard curves for plasma sialylated vitamin K-dependent protein C in the ELISA.
Colorimetric intensity and plasma vitamin K-dependent protein C concentration were related in the range of 0−10 AU/mL. Four concentrations of plasma sialylated vitamin K-dependent protein C were determined by ELISA.

were determined based on assays performed on 5 different days (two replicates of each sample per day). The within-run CV was 4.3−4.9% and the between-run CV was 4.3−5.2%.

Interference

Interference was assessed in samples containing 1.0 AU/mL sialylated vitamin K-dependent protein C. Potential interference materials were added to urine at various concentrations. There was no substantial interference from hemoglobin (up to 5000 mg/L), free bilirubin (up to 207 mg/L), ditaurobilirubin (up to 204 mg/L), chyle (up to 1400 formazine turbidity units, equal to 1176 mg/L triglyceride), ascorbic acid (up to 500 mg/L), and rheumatoid factor (up to 500 U/L).

Recovery test

To evaluate recovery in the ELISA, 0.5 and 2.0 AU/mL of recombinant Cat vitamin K-dependent protein C were added to pooled plasma (1.6 AU/mL). The percentage recovery ranged from 94.3 to 102.7%.

Sialylated vitamin K-dependent protein C levels are decreased in plasma of cats with CKD

Plasma vitamin K-dependent protein C levels and sialylated vitamin K-dependent protein C levels were mea-

sured in stage 1 CKD cats (n=50), stage 2 CKD cats (n=10) and normal control cats (n=90). Plasma vitamin K-dependent protein C values for normal control cats, stage 1 CKD cats and stage 2 CKD cats were 3.36±0.32 μg/mL, 3.46±0.31 μg/mL and 3.53±0.30 μg/mL, respectively (Fig. 3). Plasma sialylated vitamin K-dependent protein C was significantly higher in normal control cats than in stage 1 CKD cats (1.40±0.13 vs. 1.07±0.11 AU/mL, $p<0.001$), and in stage 1 CKD cats compared to stage 2 CKD cats (1.07±0.11 vs. 0.82±0.14 AU/mL, $p<0.001$) (Fig. 4). ROC curves were constructed to evaluate the cut-offs for plasma sialylated vitamin K-dependent protein C, plasma creatinine, BUN, and SDMA for distinguishing stage 1 CKD cats from normal control cats. The AUCs were 0.989 for plasma sialylated vitamin K-dependent protein C, 0.698 for plasma creatinine, 0.554 for BUN, and 0.568 for SDMA. These results suggest that plasma sialylated vitamin K-dependent protein C may be a better diagnostic stage 1 CKD biomarker than plasma creatinine, BUN and SDMA (Fig. 5). The ROC curve for plasma sialylated vitamin K-dependent protein C showed an optimal diagnostic cut-off of 1.22 AU/mL and an AUC of 0.989, with sensitivity of 97.5% and specificity of 97.5%.

Discussion

In this study, the lectin and TMT method was used to detect 18 proteins in plasma from CKD stage 1 cats and normal control cats. Sialylated vitamin K-dependent protein C was identified as the protein with the largest difference in levels between the two groups. The vitamin K-dependent protein C is synthesized in the liver in a single-chain form, and through several proteolytic steps is secreted into blood primarily as a two-chain form, containing a light chain and a heavy chain linked via a single disulfide bond[10]. Sialic acids are derivatives of the negatively charged acidic sugar neuraminic acid. Over 40 naturally occurring members of the sialic acid family have been discovered to date[11]; N-acetylneuraminic acid, N-glycolylneuraminic acid, and deaminoneuraminic acid are representative members of this family. Sialic acids usually form the terminal ends of the carbohydrate groups of glycoconjugates. All sialyltransferases characterized in animals to date, ranging from insects

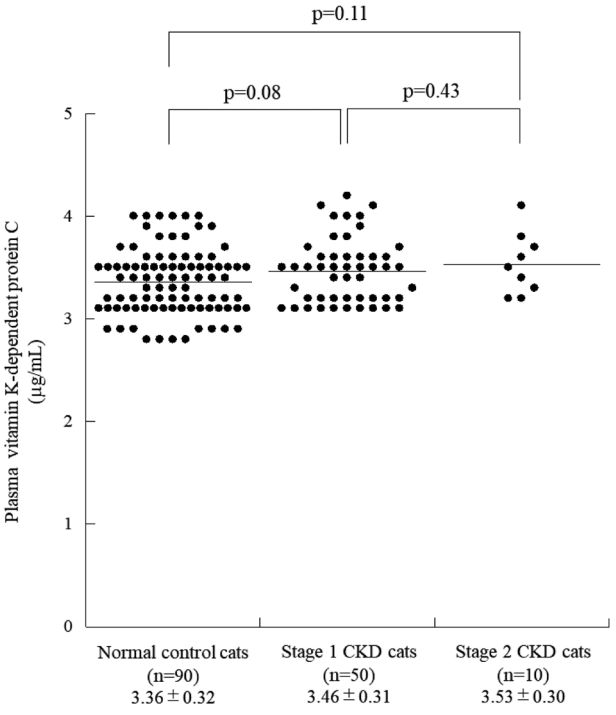

Fig. 3. Plasma vitamin K-dependent protein C levels in normal control cats and stage 1 and stage 2 CKD cats.
Plasma vitamin K-dependent protein C values for normal control cats, stage 1 CKD cats and stage 2 CKD cats were 3.36±0.32 μg/mL, 3.46±0.31 μg/mL and 3.53±0.30 μg/mL, respectively.

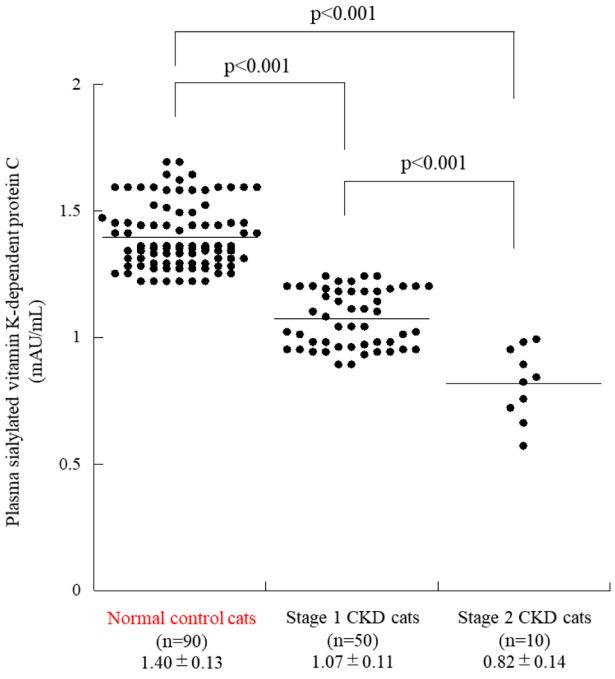

Fig. 4. Plasma sialylated vitamin K-dependent protein C levels in normal control cats and stage 1 and stage 2 CKD cats.
Plasma sialylated vitamin K-dependent protein C was significantly higher in normal control cats than in stage 1 CKD cats (1.40±0.13 vs. 1.07±0.11 AU/mL, $p<0.001$; Mann−Whitney *U*-test) and in stage 1 CKD cats compared to stage 2 CKD cats (1.07±0.11 vs. 0.82±0.14 AU/mL, $p<0.001$).

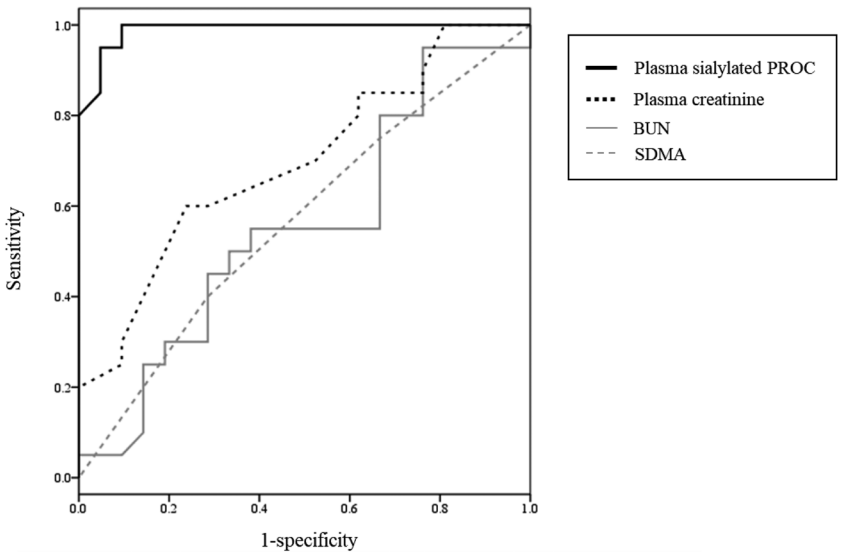

Fig. 5. Plasma sialylated vitamin K-dependent protein C is more effective than plasma creatinine, BUN and SDMA for early detection of stage 1 CKD.

ROC analyses were performed for serum levels of plasma sialylated vitamin K-dependent protein C, plasma creatinine, BUN and SDMA in stage 1 CKD and normal cats. The AUCs were 0.989 for plasma sialylated vitamin K-dependent protein C, 0.698 for plasma creatinine, 0.554 for BUN, and 0.568 for SDMA.

to mammals, feature a type II transmembrane topology and usually localize to the Golgi apparatus. The enzyme is grouped into 4 families according to the type of carbohydrate linkage they synthesize: β-galactosideα2,3-sialyltransferases (ST3Gal-I-VI), β-galactosideα2,6-sialyltransferases (ST6Gal-I and -II), GalNAcα2,6-sialyltransferases (ST6GalNAc-I−VI), and α2,8-sialyltransferases (ST8Sia-I−VI). Sialic acid was added by these enzymes[12]. During coagulation, plasma vitamin K-dependent protein C is activated by a thrombin/thrombomodulin complex[11], and in the presence of protein S, activated protein C (APC) functions as an anticoagulant by proteolytic degradation of factors Va and VIIIa[12], the only protein substrates hitherto identified for vitamin K-dependent protein C. Several animal models, including canine, bovine and feline vitamin K-dependent protein C, have been used to examine the physiological mechanisms of vitamin K-dependent protein C, and species-specific effects have been found for the anticoagulant and fibrinolytic functions of APC[13,14]. Thus, in squirrel monkeys, human APC has an anticoagulant effect, but no profibrinolytic activity[15], whereas human APC shows both anticoagulant and fibrinolytic responses in cats[16].

A decrease in vitamin K-dependent protein C has been reported in renal disease in humans, but not in cats. Patients with CKD commonly have blood coagulation disorders, and several tests can be used to measure procoagulant biomarkers in CKD[17]. Compared to normal control cats, patients with CKD have significantly higher FVII, FVIII, fibrinogen and D-dimer levels[18] and a significantly lower level of protein C. However, it has not been reported in the sialylated vitamin K-dependent protein C. Similar results were obtained in this study, with plasma sialylated vitamin K-dependent protein C found to be significantly higher in normal control cats (1.40±0.13 AU/mL) than in stage 1 (1.07±0.11 AU/mL) and stage 2 (0.82±0.14 AU/mL) CKD cats.

In this study, we showed that plasma sialylated vitamin K-dependent protein C is a potential biomarker for CKD. Various attempts have been made to identify new plasma biomarkers for CKD, and some molecular targets have been suggested as diagnostic or prognostic markers[5]. The AUC for plasma sialylated vitamin K-dependent protein C was 0.989, with sensitivity of 97.5% and specificity of 97.5%. These results suggest that plasma sialylated vitamin K-dependent protein C may be complementary to plasma creatinine, BUN and SDMA as a marker for detection of stage 1 CKD in cats. We note that the study is limited by the number of samples, and evaluation of more samples from multiple facilities is required. Longitudinal follow-up of cats in stage 1 CKD is also important to identify those with true CKD, which is progressive, and those recovering from AKI when samples were taken.

Acknowledgments

This work was supported by a Grant-in-Aid for Scientific Research (KAKENHI C: 22K07406).

Conflict of Interest

The authors declared no potential conflicts of interest with respect to the research, authorship, and/or publication of this article.

References

1) National Kidney Foundation: Board NKFKDOQIA: Clinical practice guidelines for chronic kidney disease: Evaluation, classification, and stratification IV: definition and classification of stages of chronic renal failure. *Am J Kidney Dis* 39: S46−S75, 2002.
2) Burdick MD, Schaub RG: Human protein C induces anticoagulation and increased fibrinolytic activity in the cat. *Thromb Res* 45: 413−419, 1987.
3) Colucci M, Stassen JM, Collen D: Influence of protein C activation on blood coagulation and fibrinolysis in squirrel monkeys. *J Clin Invest* 74: 200−204, 1984.
4) Comp PC, Jacocks RM, Ferrell GL, Esmon CT: Activation of protein C in vivo. *J Clin Invest* 70: 127−134, 1982.
5) Debruyn K, Haers H, Combes H, Paepe D, Peremans K, et al: Ultrasonography of the feline kidney: Technique, anatomy and changes associated with disease. *J Feline Med Surg* 14: 794−803, 2012.
6) Huang MJ, Wei RB, Wang Y, Su TY, Di P, et al: Blood coagulation system in patients with chronic kidney disease: A prospective observational study. *BMJ Open* 7: e014294, 2017.
7) King JN, Tasker S, Gunn-Moore DA, Strehlau G; BENRIC (benazepril in renal insufficiency in cats) Study Group: Prognostic factors in cats with chronic kidney disease. *J Vet Intern Med* 21: 906−916, 2007.
8) Maeda H, Igarashi K, Ishidoya M, Satoh M, Watanabe T, et al: Urinary kidney injury molecule-1 as early diagnostic marker of chronic kidney disease in cats. *Medical Mass Spectrometry* 6: 36−44, 2022.
9) Murakawa M, Okamura T, Kamura T, Kuroiwa M, Harada M, et al: A comparative study of partial primary structures of the catalytic region of mammalian protein C. *Br J Haematol* 86: 590−600, 1994.
10) Ohashi T, Igarashi Y, Mochizuki Y, Miura T, Inaba N, et al: Development of a novel fragments absorbed immunocapture enzyme assay system for tartrate-resistant acid phosphatase 5b. *Clin Chim Acta* 376: 202−212, 2007.
11) Varki A: Diversity in the sialic acids. *Glycobiology* 2: 25−40, 1992.
12) Takashima S, Tsuji S: Functional diversity of mammalian sialyltransferases. *Trends in Glycoscience and Glycotechnology* 23: 178−193, 2011.
13) Relford R, Robertson J, Clements C: Symmetric dimethylarginine: Improving the diagnosis and staging of chronic kidney disease in small animals. *Vet Clin North Am Small Anim Pract* 46: 941−960, 2016.
14) Sogawa K, Takano S, Iida F, Satoh M, Tsuchida S, et al: Identification of a novel serum biomarker for pancreatic cancer, C4b-binding protein α-chain (C4BPA) by quantitative proteomic analysis using tandem mass tags. *Br J Cancer* 115: 949−956, 2016.
15) Strickland DK, Kessler CM: Biochemical and functional properties of protein C and protein S. *Clin Chim Acta* 170: 1−23, 1987.
16) Suzuki K, Stenflo J, Dahlbäck B, Teodorsson B: Inactivation of human coagulation factor V by activated protein C. *J Biol Chem* 258: 1914−1920, 1983.
17) Syme HM, Fletcher MG, Bailey SR, Elliott J: Measurement of aldosterone in feline, canine and human urine. *J Small Anim Pract* 48: 202−208, 2007.
18) Tomura S, Saito K, Kawada K, Hirano C, Yanagi H, et al: Measurement of microalbuminuria. Comparison of the semiquantitative gold colloid dipstick method with the quantitave turbidmetric immunoassay method. *Jpn J Primary Care* 22: 37−40, 1999.
19) Tsuchida S, Satoh M, Kawashima Y, Sogawa K, Kado S, et al: Application of quantitative proteomic analysis using tandem mass tags for discovery and identification of novel biomarkers in periodontal disease. *Proteomics* 13: 2339−2350, 2013.
20) Weinsten RE, Walker FJ: Species specificity of the fibronolytic effects of activated protein C. *Thromb Res* 63: 123−131, 1991.

Short Communication

Recovery of extracellular vesicles from liquid samples using polyamine solution

Arizumi Kikuchi[1,2]*, Azumi Naruse[1], Kenichi Nonaka[1,3], Motoki Mori[2], Miyuu Yamada[2], Keiko Kano[4], Emi Mishiro-Sato[4], Kaname Tsutsumiuchi[2]

[1] Daiyukai Research Institute for Medical Science, 25 Azaicho, Ichinomiya, Aichi 491−0113, Japan
[2] College of Bioscience and Biotechnology, Chubu University, 1200 Matsumoto-cho, Kasugai-shi, Aichi 487−8501, Japan
[3] Department of Surgery, Daiyukai General Hospital, 1−9−9 Sakura, Ichinomiya, Aichi 491−8551, Japan
[4] Institute of Transformative Bio-Molecules (WPI-ITbM), Nagoya University, Furo-cho, Chikusa-ku, Nagoya 464−8601, Japan

Abstract Liquid biopsies mainly analyze nucleic acids and proteins in the free-state or extracellular vesicles (EVs) in non-solid biological samples, primarily blood. Collecting and processing liquid biopsy samples is challenging due to the large volume of samples and reagents and the need for special equipment. In a previous study, we reported a method for enriching free nucleic acids using a polyamine solution that is effective for liquid biopsy. We also investigated the reactivity of this method for EV recovery in cell culture supernatants using mass spectrometry. Samples were prepared from the cell line NCI-N87 supernatants after 48 h of culture in a serum-free medium. For comparison, samples were treated using a solution containing polyamines (PA method) or ultracentrifugation (UC method). The liquid chromatography-tandem mass spectrometry (LC-MS/MS) using the single-pot solid-phase-enhanced sample-preparation (SP3) method revealed differences between the two methods in the total ion chromatogram of the sample. However, the results of the Gene Ontology (GO) analysis showed that both methods achieved the best enrichment in GO terms related to EV. In addition, the volcano plot analysis revealed that proteins suggested to exist in EVs were distributed in areas consistent with both methods. These results indicated that the PA method can recover EV proteins in liquid samples, and their comprehensive analysis is possible using the SP3 method.

Key words: extracellular vesicles, liquid biopsy, LC-MS/MS, polyamine method, single-pot solid-phase-enhanced sample-preparation (SP3) method

Introduction

Blood samples from patients with cancer contain circulating tumor DNA (ctDNA), cell-free DNA (cfDNA), circulating tumor cells, and microRNAs (miRNAs) derived from cancer cells[1)]. Liquid biopsy is a method for the genetic and cytological analysis of these samples[1)]. It analyzed free-state nucleic acids and proteins in extracellular vesicles (EVs), including exosomes[2)]. Liquid biopsy can provide information on the nature of cancer without requiring invasive procedures associated with conventional tissue collection[3)].

EVs, including exosomes, contain proteins, mRNA, miRNA, and DNA on their surface or inside; they are stable in body fluids such as blood, urine, saliva, spinal fluid, and breast milk after being secreted from cells[4)]. EVs have attracted attention as critical biological factors that convey messages locally and remotely and are deeply involved in various diseases and biological phenomena, including cancer and immune and neurological diseases[5)]. They can be recovered using centrifugation, immunoprecipitation, particle size classification, column adsorption, or ultracentrifu-

*Corresponding author
Arizumi Kikuchi
Daiyukai Research Institute for Medical Science, 25 Azaicho, Ichinomiya, Aichi 491−0113, Japan
Tel: +81−586−533661, Fax: +81−586−533771
E-mail: akikuchi@daiyukai.or.jp
Received: February 13, 2024. Accepted: May 9, 2024.
Epub June 5, 2024.
DOI: 10.24508/mms.2024.06.006

gation[6]. Each method has different recovery rates, specificities, and the time and cost required for operation. Therefore, the method selected depends on its application. Although ultracentrifugation is considered the gold standard[7], it has limitations, such as poor recovery rates, and requires time and specialized equipment[8]. Moreover, we considered the possibility that the PA method coprecipitates EVs along with nucleic acids. In a previous study, we have devised a method for enriching free nucleic acids using polyamine-containing solutions[9].

Here, we investigated, using liquid chromatography-mass spectrometry (LC-MS/MS), whether this method can be used to recover EV proteins in cell culture supernatant.

Materials and Methods

Cell culture

For our LC-MS/MS analysis, we used a cell line, that is NCI-N87 (ATCC, Manassas, VA, USA).

The cells were cultured in RPMI-1640 with L-Glutamine and Phenol Red (Fuji film Wako, Tokyo, Japan) with 10% fetal bovine serum at 37˚C in a 5% CO^2 incubator. When the cells reached confluency, they were treated with Advanced RPMI 1640 Medium (Thermo Fisher Scientific, Waltham, MA, USA).

After 48 h of culture, the collected media were first centrifuged at 1,000×g for 10 min at room temperature (20−25˚C) to pellet and remove cells. All the centrifugation steps were performed at 4˚C. Next, the supernatant was centrifuged at 2,000×g for 20 min. The media supernatant was filtered through a 0.22-μm pore filter (HAWACH Scientific Co. LTD, Xian City, China). Each method was performed using a filtered culture medium.

Ultracentrifugation

Treated cell culture supernatant (50 mL) was used for ultracentrifugation to collect EVs. The ultracentrifugation was performed using an Optima L-90K ultracentrifuge (Beckman Colter, Fullerton, CA, USA) at 150,000×g for 100 min in a SW28.1 Roter Swinging Bucket rotor (Beckman Colter). After centrifugation, phosphate-buffered saline (PBS) was added to the top of the tube, and ultracentrifugation was performed again under the same conditions. Finally, the supernatant was removed, and the collected EVs were suspended in PBS.

Polyamine method

To begin with, 9.0 mL of the treated cell culture supernatant was transferred into a 15 mL conical centrifuge tube (Nunc, ThermoFischer Scientific, USA). Then, 1/10 volume of 5 M NaCl solution and 1/10 volume containing 0.01% Spermidine (191-13831, FUJIFILM Wako Chemicals, Osaka, Japan) were added to the tube. After the mixture was allowed to stand for 10 min at room temperature, it was centrifuged at 27,210×g (13,000 rpm) for 60 min using a micro-cooled centrifuge (Model 3700, KUBOTA CORPORATION, Tokyo, Japan). Then, the cell culture supernatant was removed and dissolved in PBS before analysis.

Mass spectrometry

Sample preparation was performed using the single-pot solid-phase-enhanced sample-preparation (SP3) technology. The protein in the sample was adjusted to 1−200 μg/mL, and dithiothreitol was added to a final concentration of 25 mM. After 30 min at room temperature, 1/10 volume of 500 mM 3-methyl-1-butanol was added and allowed to stand for 30 min at room temperature. Particles and SeraMag™ SpeedBead Carboxylate-Modified [E3] Magnetic Particles (Global Life Sciences Technologies Japan K.K., Tokyo, Japan). The bead mixture (10 μL) was added to the sample for 10 μg of protein. Then, three times the volume of ethanol was added, the sample was mixed at 1,000 rpm for 10 min at RT, and 500 μL of 80% ethanol was added, followed by washing three times using a magnetic stand. Then, 100 μL of lysyl endopeptidase plus 50 mM Tris buffer was added. After sonication, the mixture was incubated at 37˚C for 3 h. Trypsin solution was added, and the sample was mixed at 1,500 rpm at 37˚C. for 20 h. After mixing, 20% trifluoroacetic acid was added to the volume 1/20, the beads were attached to a magnetic stand, and the supernatant was collected. Then, the supernatant was desalted using GL-Tip SDB (GL Sciences Inc., Tokyo, Japan). The resulting solution was vacuum dried, and resuspended in 0.1% TFA in 2% acetonitrile to extract the peptides.

The LC-MS/MS analysis was performed using a PAL System autosampler (CTC Analytics AG, Zwingen, Switzerland) and Q Exactive Hybrid Quadrupole-Orbitrap Mass Spectrometer (Thermo Fisher Scientific). The samples were concentrated on a C18 trap column (5-μm particle size, 300 μm inner diameter, 5 mm length; Chemical Evaluation and Research Institute, Tokyo, Japan) and separated on a

C18 column (3-μm particle size, 100-μm inner diameter, 125 mm length; Nikkyo Technos, Tokyo, Japan) at a flow rate of 0.5 μL/min with an injection volume of 7.5 μL. The mobile phases were solvent A (0.5% acetic acid) and solvent B (0.5% acetic acid in 80% acetonitrile). The elution gradient for solvent B was as follows: 5% to 40% B over 100 min, then 40% to 95% B for 1 min, holding at 95% B for 3 min, then back to 5% B over 1 min, and finally re-equilibrating at 5% B for 10 min. Electrospray ionization was performed in positive-ion mode.

The instrument was operated in the DDA mode. Xcalibur 4.1.50 (ThermoFisher Scientific) was used to record peptide spectra. The full scan was acquired from 350 to 1800 *m/z* with a resolution of 17,500, automatic gain control (AGC) as 3×10^6, and maximum injection time as 60 ms. MS/MS scans were performed with a resolution of 35,000, AGC target as 1×10^5, and maximum injection time as 60 ms. The 10 highest intensity precursor ions were isolated using the quadrupole analyzer in a window of 2.0 *m/z* and fragmented by higher energy collisional dissociation (HCD) fragmentation with normalized collision energy (NCE) of 27%. Multiply-charged peptides were chosen for MS/MS experiments. Dynamic exclusion time was set to 20 s.

Data analysis

UniProt Homo Sapiens (TaxID=9606) protein sequence database downloaded on 09/24/2022 and cRAP for contaminants (http://www.thegpm.org/crap/) were used. MS/MS spectra were interpreted, and peak lists were generated using Proteome Discoverer 2.5.0.400 (ThermoFisher Scientific). Searches were performed using SEQUEST (ThermoFisher Scientific). Search parameters were set as follows: enzyme selected with two maximum missing cleavage sites, a mass tolerance of 10 ppm for peptide tolerance, 0.02 Da for MS/MS tolerance, fixed modification of carbamidomethyl (C), and variable modification of oxidation (M) and *N*-terminal acetylation. Peptide identifications were based on significant Xcorr values (high confidence filter). Peptide identification and modification information returned from SEQUEST were filtered at a false discovery rate (FDR) of 1% using the Percolator node of Proteome Discoverer to obtain confirmed peptide identification and modification lists of HCD MS/MS. The LC-MS/MS data generated in this study have been deposited in jPOST repository database (project ID, JPST001807, accession ID, PXD035832)[10].

Furthermore, we used the proteins described in MISEV2018[6] and examined the validity of the proteins detected. Among the proteins listed, we identified peptide spectrum matches (PSM) for significant proteins. We also examined the correlation between the two methods using this data.

We also examined the properties of the PA and UC methods using total ion chromatogram, diagrams, and volcano plot, mainly to characterize the recovered peptides. The volcano plot was also used to examine both methods' agreement rate and characteristics of the proteins detected. Volcano plots were created with a fold change value (log2) greater than or equal to 1.5 and a p-value of 0.05>. The method's relative standard deviation (RSD) was determined and reproducibility was discussed. RSD was calculated by finding the mean and SD of the PSMs listed in Table 1.

We performed Go Ontology (GO) analysis on cellular component categories using proteins detected by both methods for PSMs with a mean of 4 or higher. The analysis used the DAVID open-source program, v2024q1[11,12].

Results

Table 1 shows the protein data obtained by both methods, using the detection data for the content described in MISEV2018 as protein content-EV characterization, and summarized for those with PSMs of 4 or higher. Using PSMs, a correlation coefficient of R=0.765 was obtained for both methods, resulting in an overall positive correlation in Fig. S1. In addition, results for all proteins listed in MISEV2018 are represented in Table S1.

Fig. 1A shows the total ion chromatograms. Although the same samples were treated using PA and UC methods, each method showed a different profile.

Fig. 1B show the results of the volcano plot for each method. Fig. 1B shows the markers CD9, CD63, CD81, and Flotillin-1, which were considered particularly important in EVs. The PA method identified common proteins believed to be contained in EVs near the origin. Table S2 presents the list of proteins with quantitative information used in the analysis.

Table S3 summarizes the number and percentage of proteins with different reproducibility based on the RSD values of PSMs in proteomics using PA and UC methods. About 80% of the proteins detected with the PA method have a smaller RSD value than 30%, whereas about 20% of the

Table 1. Protein content by LC-MS/MS

Description	Gene Symbol	PSMs			
		(a)		(b)	
		Mean	S.D.	Mean	S.D.
Integrin alpha-2	ITGA2	4.0	2.0	3.7	2.3
Integrin beta-3	ITGB3	6.7	1.2	4.5	0.7
HLA class I histocompatibility antigen, C alpha chain	HLA-C	9.0	1.7	8.7	6.1
Integrin alpha-6	ITGA6	10.3	0.6	9.0	8.0
Integrin beta-1	ITGB1	13.7	1.5	12.0	5.3
HLA class I histocompatibility antigen, A alpha chain	HLA-A	16.3	1.2	15.3	11.9
HLA class I histocompatibility antigen, B alpha chain	HLA-B	16.3	1.5	18.7	11.0
Integrin beta-4 OS=Homo sapiens	ITGB4	18.7	4.9	15.0	12.1
Syndecan-4 OS=Homo sapiens	SDC4	45.3	5.7	5.5	2.1
CD9 antigen OS=Homo sapiens	CD9	6.7	1.2	5.0	4.0
Receptor tyrosine-protein kinase erbB-2	ERBB2	22.0	1.7	24.3	16.0
Charged multivesicular body protein 1b	CHMP1B	4.0	1.0	6.3	4.0
Annexin A7 OS=Homo sapiens	ANXA7	1.3	0.6	4.0	1.4
ADP-ribosylation factor 6	ARF6	1.7	1.2	4.5	0.7
Flotillin-2	FLOT2	1.7	1.2	6.5	0.7
EH domain-containing protein 2	EHD2	3.7	1.2	5.5	3.5
Transforming protein RhoA	RHOA	4.0	0.0	6.7	3.8
Flotillin-1	FLOT1	4.0	1.0	7.0	5.3
Annexin A13	ANXA13	5.0	1.0	13.5	4.9
Charged multivesicular body protein 2b	CHMP2B	5.7	1.5	5.0	4.0
Arrestin domain-containing protein 1	ARRDC1	5.7	1.5	7.3	4.7
Charged multivesicular body protein 1a	CHMP1A	7.3	1.5	9.3	6.4
EH domain-containing protein 3	EHD3	8.0	0.0	8.3	6.7
Vacuolar protein sorting-associated protein 4A	VPS4A	8.0	3.0	12.5	4.9
Charged multivesicular body protein 3	CHMP3	8.3	3.8	12.7	9.3
Annexin A4	ANXA4	9.7	1.5	14.3	10.7
Tumor susceptibility gene 101 protein	TSG101	10.0	1.7	13.3	9.3
Charged multivesicular body protein 4b	CHMP4B	12.0	1.7	19.7	11.0
Vacuolar protein sorting-associated protein 4B	VPS4B	12.7	4.0	14.7	11.1
Charged multivesicular body protein 4c	CHMP4C	12.7	1.5	17.3	8.1
Annexin A3	ANXA3	16.3	0.6	12.3	6.4
EH domain-containing protein 4	EHD4	18.0	3.0	17.0	14.1
Annexin A1	ANXA1	21.3	1.2	18.0	8.5
Programmed cell death 6-interacting protein	PDCD6IP	23.7	1.5	34.7	23.2
Charged multivesicular body protein 2a	CHMP2A	26	2.6	45.7	28.7
EH domain-containing protein 1	EHD1	26.7	3.2	23.7	22.1
Putative annexin A2-like protein	ANXA2P2	50.3	3.2	42	18.1
Annexin A2	ANXA2	67.7	3.1	59.3	25
Syntenin-1	SDCBP	5.0	1.0	10.0	4.2
Annexin A11 OS=Homo sapiens	ANXA11	11.0	2.0	12.0	5.3
Glyceraldehyde-3-phosphate dehydrogenase	GAPDH	4.0	0.0	4.7	4.0
Actin, cytoplasmic 1	ACTB	61.0	2.6	49.0	32.8
Tubulin beta-3 chain	TUBB3	2.5	2.1	4.0	4.2
Tubulin beta-8 chain	TUBB8	2.7	1.5	4.5	4.9
Tubulin beta-2B chain	TUBB2B	2.7	1.2	7.5	6.4
Tubulin alpha-4A chain	TUBA4A	3.3	1.2	5.0	6.1
Tubulin alpha-3E chain	TUBA3E	4.0	1.0	5.0	5.7
Tubulin alpha-3D chain	TUBA3D	4.0	1.0	5.5	6.4
Tubulin beta chain	TUBB	4.3	0.6	9.0	5.7
Tubulin alpha-1A chain	TUBA1A	4.7	1.5	8.5	10.6
Tubulin alpha-1B chain	TUBA1B	4.7	1.5	9.5	12.0
Tubulin alpha-1C chain	TUBA1C	4.7	1.5	9.5	12.0
Tubulin beta-4B chain	TUBB4B	6.0	1.0	6.3	6.1
Tubulin beta-2A chain	TUBB2A	2.7	1.2	8.0	7.1
Heat shock protein HSP 90-beta	HSP90AB1	32.0	5.3	22.0	14.2
Heat shock cognate 71 kDa protein	HSPA8	39.3	4.7	43.0	27.1
Albumin	ALB	67.7	18.5	12.0	12.2

(a) PA method and (B) UC method. The analysis was performed with N=3, and the list was made up of PSMs obtained by any of the methods with a mean of 4 or higher (PSMs, peptide spectrum matches; SD, standard deviation).

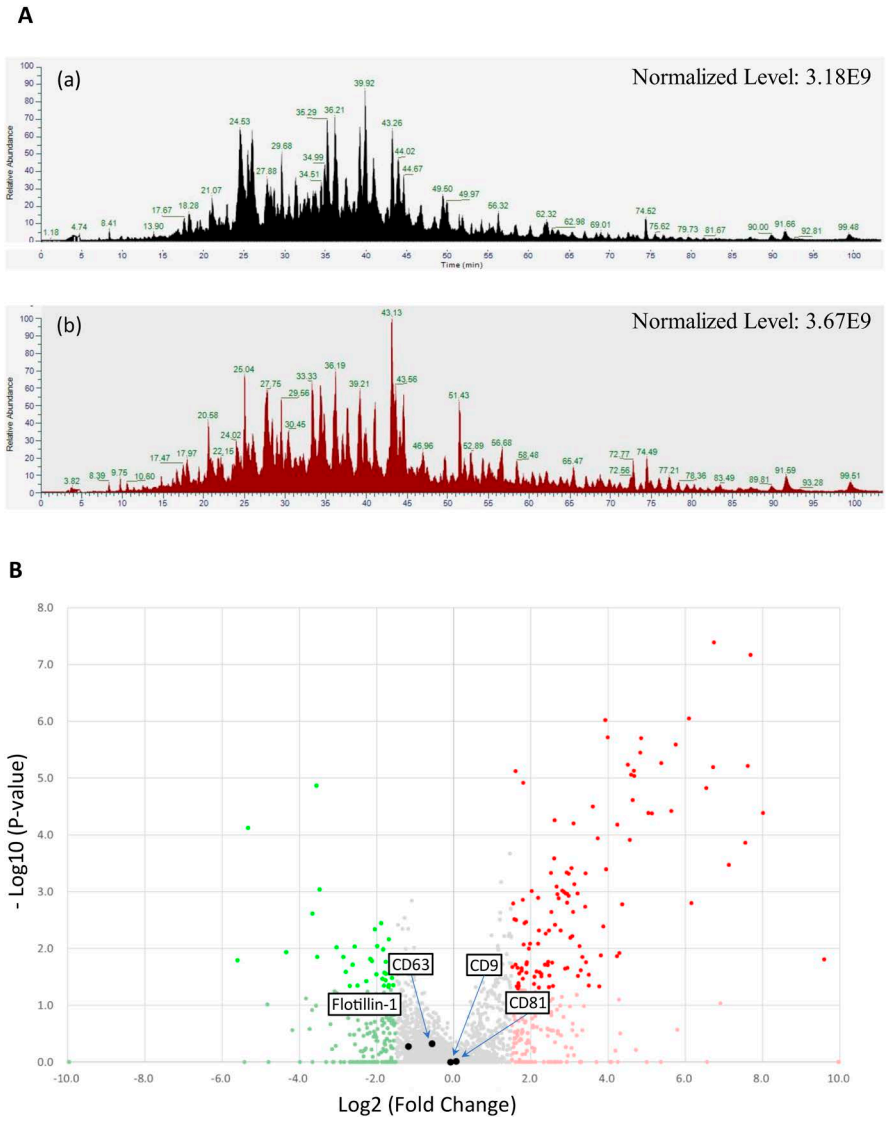

Fig. 1. Comparison of both methods using total ion chromatogram and volcano plot.

A. Total ion chromatogram for each method. (a) PA method, (b) UC method. B. Volcano plot for each method. Marked for proteins in EVs at NCI-N87. Created using abundance data obtained by LC-MS/MS. The x-axis indicates log2 fold change for each gene, and y-axis indicates -log10 p-value. Red dots indicate proteins with p-values <0.05, and green dots indicate proteins with p-values ≥ 0.05. The significance of differences was evaluated by t-test, with p-value <0.05 being significant.

proteins with the UC method.

In the GO analysis, EV markers, including exosomes, dominated the highest annotation cluster with enrichment. The enrichment scores for the PA and UC methods were 206.6 and 233.6, respectively (Table S4 A, B) .

Furthermore, information regarding cellular components obtained in this analysis is described in Fig. S2.

Discussion

Cancer is the leading cause of death worldwide; therefore, early cancer detection and appropriate treatment are crucial[13]. Usually, cancer is diagnosed by tissue biopsy; however, the invasive sampling and inability to accurately capture tumor dynamics owing to the heterogeneous distribution of tumor cells imposes challenges to cancer diagnosis[14]. Meanwhile, liquid biopsy is a promising method to address these challenges. In addition, liquid biopsy results have recently been used to administer companion diagnostic agents.

We compared the EVs obtained by PA and UC methods using the LC-MS/MS. Together with the UC method, LC-MS/MS detected proteins that indicate EVs according to the categories in the MISEV2018. The total ion chromatograms obtained using the PA method differed from those obtained using the UC method. In the analysis with the volcano plot, the common markers that were supposed

to be present in the EV appeared relatively close to the origin. However, their distribution showed different patterns.

Although the UC method is the standard method for EV recovery, it simultaneously recovers impurities such as vesicles and proteins other than EVs, resulting in lower purity of EVs[8]. These factors may have influenced the differences observed between the two methods in the present study. In addition, EVs contain exosomes, microvesicles, and apoptotic bodies, and the reactivity of each substance in each method[15], including PA method, can significantly affect the results.

The proteins detected by both methods are positively correlated and show a similar trend in detecting EV-related markers. Furthermore, we believe the PA method is less susceptible to contamination by dead cells. The results of the GO analysis also suggest that this is an efficient method of recovering EV-related substances. Although the PA method has shown recovery of proteins in EVs, its characteristics will need to be clarified through further studies.

Polyamines are involved in cell growth and survival, autophagy[16], and the onset and progression of neurological disease[17]. Additionally, a link between polyamine metabolic pathways and cancer has been reported[18]. Polyamines include streptomycin, spermidine, and spermine, which exist in cells at a level of several millimolar concentrations[19]. Moreover, polyamines are polycationic molecules[20], which is the characteristic the PA method focuses on.

This method can recover cell-free nucleic acids and EVs using polyamine-containing solutions[9], which we believe is due to the formation of ion complexes between polyamines and these substances with negative charges on the surface. Furthermore, under high salt concentration conditions, substances with small particle sizes and low charge density do not lead to the formation of coacervate[21], which may also affect not recovering a variety of free proteins.

The PA method does not require special equipment, is relatively easy to operate, and is low-cost. In addition, a pretreatment is possible when further downstream purification or nucleic acid extraction is performed on samples collected using the PA method. Regarding the reproducibility of the PA method, approximately 80% of the proteins detected in this study showed RSD within 30%. Maintaining and improving reproducibility is an essential issue in analysis. We believe that attention should be paid not only to technical proficiency but also to further simplifying the process.

Liquid biopsy has been reported in urine, saliva, cerebrospinal fluid, and stool other than blood[22], and is expected to be used in actual clinical practice. Free nucleic acids and proteins in the samples used in liquid biopsies are often present at low concentrations[23] and require a large sample volume. In addition, large amounts of reagents and special equipment are required. However, because the PA method can be enriched, it is possible to use ordinary processing reagents to handle enriched samples.

We have demonstrated the presence of protein markers in the characterization shown in MISEV2018 using the PA method; however, it is unclear to what extent the exosomes in EVs were recovered in this study. Furthermore, we believe that a comparative study of this point using methods other than the UC method should be conducted. Therefore, we are currently examining this point using various analytical methods.

The cargo of tumor-derived EVs is consistent with the genetic content of parent tumor cells[24]. Therefore, the cargo contained in the EVs has attracted attention as a new biomarker for cancer diagnosis and prognosis prediction[25]. Moreover, EVs are stable in body fluids, and the cargo in the EVs is protected from degradation[26,27]. Therefore, EVs are of interest as excellent biological components for liquid biopsy[1,28]. We are currently conducting various studies focusing on its application in liquid biopsy. We believe that the PA method can potentially demonstrate a broad utility by comparing its performance with that of other methods for EV recovery.

Mass spectrometry is being implemented in various ways in the medical field because of its ability for comprehensive analysis and its excellent sensitivity and specificity. We believe that this method will be an effective method in clinical testing of liquid biopsy samples.

Conclusions

EV analysis using LC-MS/MS with the SP3 method was also feasible. The LC-MS/MS results showed that the PA method can detect peptides with EV properties.

Conflict of Interest

The authors declare no competing interests.

Additional Information

The results of this study are organized in the text or in

supplementary materials.

References

1) Vaidyanathan R, Soon RH, Zhang P, Jiang L, Lim CT: Cancer diagnosis: From tumor to liquid biopsy and beyond. *Lab Chip* 19: 11−34, 2018.
2) Pantel K, Alix-Panabières C: Circulating tumour cells in cancer patients: Challenges and perspectives. *Trends Mol Med* 16: 398−406, 2010.
3) Jelski W, Mroczko B: Molecular and circulating biomarkers of gastric cancer. *Int J Mol Sci* 23: 2022.
4) Raposso G, Stoorovogel W: Extracellular vesicles; exosomes, microvesicles, and friends. *J Cell Biol* 200: 373−383, 2013.
5) Yáñez-Mó M, Siljander PR-M, Andreu Z, Zavec AB, Borràs FE, et al: Biological properties of extracellular vesicles and their physiological functions. *J Extracell Vesicles* v4: 27066, 2015.
6) Théry C, Witwer KW, Aikawa E, Alcaraz MJ, Anderson JD, et al: Minimal information for studies of extracellular vesicles 2018 (MISEV2018): A position statement of the International Society for Extracellular Vesicles and update of the MISEV2014 guidelines. *J Extracell Vesicles* 7: 1535750, 2018.
7) Royo F, Théry C, Falcón-Pérez JM, Nieuwland R, Witwer KW: Methods for separation and characterization of extracellular vesicles: Results of a worldwide survey performed by the ISEV rigor and standardization subcommittee. *Cells* 9: 1955, 2020.
8) Zhang H, Freitas D, Kim HS, Fabijanic K, Li Z, et al: Identification of distinct nanoparticles and subsets of extracellular vesicles by asymmetric flow field-flow fractionation. *Nat Cell Biol* 20: 332−343, 2018.
9) Kikuchi A: Japan Patent Kokai 2022−86551.
10) Okuda S, Watanabe Y, Moriya Y, Kawano S, Yamamoto T, et al: jPOSTrepo: an international standard data repository for proteomes. *Nucleic Acid Res* 45(D1): D1107−D1111, 2017.
11) Sherman BT, Hao M, Qiu J, Jiao X, Baseler MW, et al: DAVID: A web server for functional enrichment analysis and functional annotation of gene lists (2021 update). *Nucleic Acid Res* 50(W1): W216−W221, 2022.
12) Dennis GJ, Sherman BT, Hosack DA, Yang J, Gao W, et al: DAVID: Database for annotation, visualization, and integrated discovery. *Genome Biol* 4: P3, 2003.
13) Hughes CS, Moggridge S, Müller T, Sorensen PH, Morin GB, et al: Single-pot, solid-phase-enhanced sample preparation for proteomics experiments. *Nat Protoc* 14: 68−85, 2019.
14) Sung H, Ferlay J, Siegel RL, Laversanne M, Soerjomataram, et al: Global cancer statistics 2020: GLOBOCAN estimates of incidence and mortality worldwide for 36 cancers in 185 countries. *CA Cancer J Clin* 71: 209−249, 2021.
15) Sala M, Ros M, Saltel F: A complex and evolutive character: Two face aspects of ECM in tumor progression. *Front Oncol* 10:1620, 2020.
16) Zhou X, Xie F, Wang L, Zhang L, Zhang S, et al: The function and clinical application of extracellular vesicles in innate immune regulation. *Cell Mol Immunol* 17: 323−334, 2019.
17) Minarini A, Zini M, Milelli A, Tumiatti V, Marchetti C, et al: Synthetic polyamines activating autophagy: Effects on cancer cell death. *Eur J Med Chem* 67: 359−366, 2020.
18) Saiki S, Sasazawa Y, Fujimaki M, Kamagata K, Kaga N: A metabolic profile of polyamines in parkinson disease: A promising biomarker. *Ann Neurol* 86: 251−263, 2019.
19) Casero Jr RA, Stewart TM, Pegg TE: Polyamine metabolism and cancer: Treatments, challenges and opportunities. *Nat Rev Cancer* 18: 681−695, 2018.
20) Madeo F, Eisenberg T, Pietrocola F, Kroemer G: Spermidine in health and disease. *Science* 359: 6387, 2018.
21) Tsutsumiuchi K, Aoi K, Okada M: Ion complex formation between poly(amido amine) dendrimer HCl salt and poly(L-glutamic acid) sodium salt. *Polym J* 32: 107−112, 2000.
22) Firpo MR, Mounce BC: Diverse functions of polyamines in virus infection. *Biomolecules* 10: 628, 2020.
23) Peng M, Chen C, Hulbert A, Brock MV, Yu F: Non-blood circulating tumor DNA detection in cancer. *Onco Target* 8: 69162−69173, 2017.
24) Koukourakis IM, Xanthopoulou E, Koukourakis MI: Using liquid biopsy to predict relapse after radiotherapy in squamous cell head neck and esophageal cancer. *Cancer Diagn Progn* 3: 403−410, 2023.
25) Tovar‐Camargo OA, Toden S, Goel A: Exosomal microRNA biomarkers: Emerging frontiers in colorectal and other human cancers. *Expert Rev Mol Diagn* 16: 553−567, 2016.
26) Fu M, Gu J, Jiang P, Qian H, Xu W, Zhang X: Exosomes in gastric cancer: Roles, mechanisms, and applications. *Mol Cancer* 18: 41, 2019.

27) Baassiri A, Nassar F, Mukherji D, Shamseddine A, Nasr R, et al: Exosomal noncoding RNA in liquid biopsies as a promising bio marker for colorectal cancer. *Int J Mol Sci* 21: 1398, 2020.
28) Kosaka N, Iguchi H, Yoshioka Y, Takeshita F, Matsuki Y, et al: Secretory mechanisms and intercellular transfer of microRNAs in living cells. *J Biol Chem* 285: 17442−17452, 2010.
29) Li S, Yi M, Dong B, Tan X, Luo S, et al: The role of exosomes in liquid biopsy for cancer diagnosis and prognosis prediction. *Int J Cancer* 148: 2640−2651, 2021.

Medical Mass Spectrometry Vol. 8 No. 1, 2024

Publication Date: June 25, 2024
Publisher: Japanese Society for Biomedical Mass Spectrometry
6 Nikko-cho, Ichinomiya, Aichi 491−0938, Japan
Shubun University
Instructions for Authors: http://www.jsbms.jp/english/doc/inst_en.pdf
Printer: International Academic Publishing Co., Ltd.